An activity model for phase equilibria in the H_2O-CO_2-NaCl system

Benoît Dubacq[a], Mike J. Bickle[a], Katy A. Evans[b]

[a] *Dept. of Earth Sciences, University of Cambridge, Downing Street, Cambridge, CB2 3EQ, UK, bd298@cam.ac.uk, Phone +44 (0)1223 333485.*

[b] *Dept. Applied Geology, Curtin University of Technology, GPO Box U1987 Perth, WA 6845, Australia*

Abstract

We present a semi-empirical thermodynamic model with uncertainties that encompasses the full range of compositions in H_2O-CO_2-NaCl mixtures in the range of 10-350°C and 1-3500 bars. For binary H_2O-CO_2 mixtures, the activity-composition model is built from solubility experiments. The parameters describing interactions between H_2O and CO_2 are independent of the absolute thermodynamic properties of the end-members and vary strongly non-linearly with pressure and temperature. The activity of water remains higher than 0.88 in CO_2-saturated solutions across the entire pressure-temperature range. In the H_2O-NaCl system, it is shown that the speciation of aqueous components can be accounted for by a thermodynamic formalism where activities are described by interaction parameters varying with intensive properties such as pressure and temperature but not with concentration or ionic strength, ensuring consistency with the Gibbs-Duhem relation. The thermodynamic model reproduces solubility experiments of halite up to 650°C and 10 kbar, and accounts for ion pairing of aqueous sodium and chloride ions with the use of associated and dissociated aqueous sodium chloride end-members whose relative proportions vary with salinity. In the H_2O-CO_2-NaCl

system, an activity-composition model reproduces the salting-out effect with interactions parameters between aqueous CO_2 and the aqueous species created by halite dissolution. The proposed thermodynamic properties are compatible with the THERMOCALC database (Holland and Powell, J.M.G., 2011, 29, 333-383) and the equations used to retrieve the activity model in H_2O-CO_2 can be readily applied to other systems, including minerals.

Keywords: Fluid-rock interactions, activity-composition model, H_2O - CO_2 - NaCl, CO_2 solubility, minerals solubility, speciation, thermodynamics, salting-out effect, Carbon Capture and Storage, Enhanced Oil Recovery, water activity

---

1. INTRODUCTION

Fluids play a key role in the evolution of the lithosphere, at the surface (e.g. Nesbitt and Markovics, 1997; Tipper et al., 2006), where crust is created at subduction zones (e.g. Tatsumi, 1989; Hacker et al., 2003) as well as in the deep crust and upper mantle (Newton et al., 1980; Thompson, 1992), in seawater composition (Edmond et al., 1979), seismicity (Chester et al., 1993), mantle dynamics (Molnar et al., 1993), exhumation of subducted material (Angiboust et al., 2012), ore deposits (e.g. Wilkinson and Johnston, 1996, for H_2O-CO_2-NaCl) and melting (White et al., 2001). Aqueous solutions transform their host rock by dissolution - precipitation reactions and ion exchange, transporting geochemical fluxes and changing rock properties.

Concern about the environmental impacts of greenhouse gases emissions has created an interest in geological carbon storage where safe, long-term storage will require prediction of reactions between CO_2, aqueous formation fluids and reser-

voir minerals (Bickle, 2009; Wigley et al., 2012). Understanding the behavior of mixed H_2O-CO_2 fluids is also important for modeling the global carbon cycle and estimating metamorphic CO_2 fluxes (Kerrick and Caldeira, 1998; Becker et al., 2008).

Thermodynamic calculations can be used to predict the behaviour of, and to interpret processes within, fluid - rock systems. Such calculations require knowledge of the thermodynamic properties of end-member minerals, fluids, and solutes, as well as activity-composition relationships, which describe the thermodynamic properties of mixtures as a function of their composition. The thermodynamic properties of mineral and fluid end-members are relatively well known (e.g. Holland and Powell, 1998; Evans et al., 2010; Holland and Powell, 2011). However, replication of observed fluid properties by activity-composition expressions, particularly for salt-rich, mixed solvent fluids at pressure-temperature conditions where liquid and gas phases coexist, and close to the critical point, has proved more challenging. Such fluids are of intense interest for geological applications, particularly sequestration of CO_2 and the extraction of geothermal energy.

A number of workers have developed activity-composition relationships for fluids that are salt-rich and/or mixed solvent and/or mixed phase or close to the critical point (e.g Helgeson et al., 1981; Pitzer, 1973; Pitzer and Mayorga, 1973; Pitzer and Simonson, 1986; Chapman et al., 1989; Clegg and Pitzer, 1992; Clegg et al., 1992; Duan and Sun, 2003; Ji et al., 2005; Duan et al., 2006; García et al., 2006; Ji and Zhu, 2012). These models perform well in the regions of pressure - temperature - composition space for which they are designed. However, there is still a need for a model that:

1. replicates available data for mixed phase, salt-rich, mixed-solvent fluids

close to the critical end point;

2. allows realistic propagation of uncertainties;
3. allows dissociation of ionic solutes such as NaCl;
4. can be extended readily to more complex systems as calibration data becomes available;
5. is compatible with existing thermodynamic databases and software. Mineral phases in fluid-rock systems in CO_2 sequestration and geothermal environments have a strong influence on fluid compositions via fluid-rock reaction, and almost always involve phases with complex activity-composition relationships such as ternary carbonates and feldspars. At this time, there is no software capable of combining the most recent and sophisticated activity-composition models for fluids *and* mineral phases.
6. is based on a relatively small number of fitted parameters; minimisation of the number of parameter facilitates fit for systems where the data is sparse;
7. is based on physically realistic expressions with a minimum reliance on empirical expressions such as power-law series. Such an approach increases the ability of a model to extrapolate beyond the limits of experimental data.

In this paper, we utilise the the Debye-Huckel ASymmetric Formalism (DHASF) model developed by Evans and Powell (2006) to describe activity-composition relations between H_2O-CO_2-NaCl in mixed solvent fluids in the two phase field and close to the critical point. The model is compatible with the computer program THERMOCALC, which utilises a large, internally consistent database and incorporates the facility for error propagation and for complex activity-composition calculations in fluids and mineral phases. First, phase diagrams are constructed with the ASF model applied to the binary mixture of water and carbon dioxide.

Then the DH-ASF model is parameterized to reproduce experimental results of halite solubility in water, taking the pairing of aqueous Na^+ and Cl^- into account. Finally, the effect of aqueous NaCl on CO_2 solubility is fitted in the H_2O-CO_2-NaCl system. The choice of the H_2O-CO_2-NaCl chemical system is dictated by its geological importance and the large number of experimental results available. The approach is designed to be readily extended to additional end-members as such data becomes available.

2. TERMINOLOGY

In the following, we use end-members for components, defined as the smallest set of chemical formulae needed to describe the composition of all the phases in the system (Anderson and Crerar, 1993; Spear, 1993). We model thermodynamic equilibrium and the phases considered here are assumed to be chemically and physically homogeneous substances bounded by distinct interfaces with adjacent phases and may be minerals exhibiting solid-solutions, melts, aqueous liquids, gases or supercritical fluids.

A key to all symbols is provided in Table 1.

3. THERMODYNAMIC BACKGROUND

The Debye-Hückel limiting law (Debye and Hückel, 1923a,b) and its extensions (e.g. Helgeson et al., 1981) have been extensively used to calculate the thermodynamic properties of aqueous species for geological applications but are restricted to ionic strengths below 0.1 molal, whereas solutions of interest such as sedimentary brines and metamorphic fluids have often higher ionic strengths.

The Pitzer model (Pitzer, 1973; Pitzer and Mayorga, 1973; Pitzer and Simonson, 1986; Clegg and Pitzer, 1992; Clegg et al., 1992) has provided a framework

to express the activity coefficient, γ, of aqueous species at higher ionic strengths and can be applied to salt-bearing solutions from infinite dilution to fused salt mixtures. This large range of concentrations is accounted for by an activity model describing a short-range force term for highly-concentrated solutions, with interaction parameters fitted to a convenient expression such as a Margules expansion (e.g., Pitzer and Simonson, 1986), to which is added a Debye-Hückel term resulting from long-range ionic forces which dominate at low concentrations. However, the Pitzer models cannot be used to describe solutions at temperatures and pressures much different to those of the original calibration, or to calculate the properties of mixed-solvent solutions.

A different approach has been suggested by Duan et al. (2006) who proposed an activity model to calculate the solubility of CO_2 in aqueous fluids by mapping variations of the fugacity coefficient ϕ_{CO_2} in the two-phase mixture. ϕ_{CO_2} is linked to the activity of CO_2 in the mixture, a_{CO_2}, such as $a_{CO_2} = \frac{\phi_{CO_2}}{\phi^0_{CO_2}} X_{CO_2}$, where $\phi^0_{CO_2}$ is the fugacity coefficient of CO_2 in its pure phase and X_{CO_2} the mole fraction of CO_2 in the gas phase (Flowers, 1979). The ratio $\frac{\phi_{CO_2}}{\phi^0_{CO_2}}$ is the activity coefficient γ_{CO_2} (e.g., Holland and Powell, 2003). Duan and Sun (2003) note that ϕ_{CO_2} differs very little from $\phi^0_{CO_2}$ at temperatures between 0 and 260°C for all pressures lower than 2kbar, and subsequently assume them to be equal so that $\gamma_{CO_2} = 1$ and $a_{CO_2} = X_{CO_2}$. Duan et al. (2006) have extended this assumption to a mixing scheme where ϕ_{CO_2} is only a function of pressure and temperature. However it is incorrect at conditions close to the closure of the H_2O-CO_2 solvus because experimental results imply $\gamma_{CO_2} \neq 1$ (e.g. Todheide and Franck, 1963). We show below that $\gamma_{CO_2} = 1.07$ at 100°C - 1bar and $\gamma_{CO_2} = 1.35$ at 260°C - 2kbar.

Furthermore, assumptions in Duan and Sun (2003) reduce the chemical po-

tential of CO_2 in the gas phase ($\mu^v_{CO_2}$) to $\mu^v_{CO_2}(P,T,y) = \mathrm{R}T\ln(P - P_{H_2O}) + \mathrm{R}T\ln(\phi^0_{CO_2})$, where y is amount of CO_2 in the gas phase, T is temperature, P is pressure, and P_{H_2O} is boiling pressure for pure water at T. This is erroneous because 1) it assumes that CO_2 has no enthalpy of formation and 2) it describes $\mu^v_{CO_2}$ as independent of the composition of the mixture but sensitive to P_{H_2O}, even when the composition tends towards pure CO_2. This model also has the disadvantages that little information is provided on the activity of water in the mixture.

SAFT (Statistical Associating Fluid Theory, Chapman et al., 1989) equations of state (EOS) can be altered to describe variations of ϕ_{CO_2} and have been shown by Ji et al. (2005) and Ji and Zhu (2012) to reproduce well the experimentally-derived solubility and density of H_2O-CO_2 mixtures to which their short-range parameters are fitted over the range 20-200°C and 1-600 bars. However their predictive power is not greater than other semi-empirical, simpler models.

Oelkers et al. (2009) highlighted the importance of using internally consistent thermodynamic databases in geochemical modeling. Research in metamorphic petrology has produced reliable internally consistent thermodynamic databases, amongst which the regularly updated databases of THERMOCALC (Holland and Powell, 1998; Powell et al., 1998; Holland and Powell, 2003, 2011) and TWEEQ (Berman, 1988; Berman and Aranovich, 1996; Aranovich and Berman, 1996) provide thermodynamics properties for more than 150 minerals of petrological interest each.

3.1. The ASF model

In this study, we use the ASF model developed by Holland and Powell (2003) and its extension for aqueous species (DH-ASF, from Evans and Powell, 2006). ASF and DH-ASF are frameworks for activity-composition models used in the

THERMOCALC software together with its internally consistent database, where enthalpies of formation of various end-members at standard state and their uncertainties have been estimated from calorimetric measurements and phase equilibria.

The DH-ASF model of Evans and Powell (2006) is an extension for aqueous species of the ASF model. DH-ASF shares fundamental similarities with Pitzer models in that it adds a short-range force term (described by ASF) to a Debye-Hückel term to express the excess Gibbs energy of a mixture. DH-ASF and ASF both use standard states where the considered component is in its pure phase ($x = 1$) and has unit activity at any pressure and temperature. For aqueous species, DH-ASF includes components for which thermodynamic data are derived from dilute solutions and therefore their standard state is always hypothetical. A schematic representation of the variations of the chemical potential of an aqueous species with concentration is shown in appendix A together with the standard state used here and the usual 1M standard state. Details of the method are described by Evans and Powell (2006) and the corresponding codes have been made available by Evans and Powell (2007).

With this method, it is possible to model mixed solvent fluids because no distinction is made between constituents forming both co-solvents and what would be traditionally viewed as a solute, such as CO_2, in which case the concept of solvent and solutes becomes restrictive. The method uses mean ionic compounds to describe aqueous species. For charged species such as $\mathrm{A}^{\mathrm{n}+}$ and $\mathrm{B}^{\mathrm{m}-}$, mean ionic compounds are obtained by summing cations and anions to form $\mathrm{m} + \mathrm{n}$ hypothetical neutral species $(\mathrm{A_mB_n}\pm)_{1/(\mathrm{m+n})}$. The stoichiometric factor of $1/(\mathrm{m} + \mathrm{n})$ ensures that the calculated number of moles present in solution is correct, which is important for the entropy contributions to the free energy. This also ensures

198 the electro-neutrality of the mixture and allows a simple description of ion pairing
199 and common ion effects.

200 The thermodynamic properties of mean ionic compounds are calculated from
201 the sum of the properties of their constituents and extrapolated to standard state at
202 unit mole fraction as shown in appendix A.

203 The chemical potential of an end-member l in a solution can be expressed as:

$$\mu_l(x_l) = \mu_l^0 + \mathrm{R}T\log(x_l) + \mathrm{R}T\log(\gamma_l) \tag{1}$$

204 where R is the ideal gas constant, T is temperature, μ_l is the chemical potential
205 of l, μ_l^0 the chemical potential of l at standard pressure and temperature, x_l is the
206 mole fraction of l and γ_l the activity coefficient of l. With the ASF formalism
207 of Holland and Powell (2003), a single activity-composition model constrains the
208 activities of the two end-members in the two phases along a binary mixture. The
209 activity coefficient γ of l in a system with n end-members is expressed as:

$$\mathrm{R}T\log(\gamma_l) = -\sum_{i=1}^{n-1}\sum_{j>i}^{n} q_i q_j W_{ij}^* \tag{2}$$

210 where i and j are end-members of the mixture, $q_i = 1 - \Phi_i$ when $i = l$, and
211 $q_i = -\Phi_i$ when $i \neq l$ where Φ_i and W_{ij}^* are the size parameter-adjusted proportion
212 and interaction energy defined respectively as:

$$\Phi_i = \frac{x_i\alpha_i}{\sum_{j=1}^{n} x_j\alpha_j} \tag{3}$$

213

$$W_{ij}^* = W_{ij}\frac{2\alpha_l}{\alpha_i + \alpha_j} \tag{4}$$

214 W_{ij} describes the magnitude of the excess Gibbs free energy function in terms of
215 the parameters α_l attributed to each end-member. This model yields the following

expression for the excess Gibbs energy $\overline{G}^{\text{xs}}_{\text{m}}(x)$ of a mixture comprised of n end-members:

$$\overline{G}^{\text{xs}}_{\text{m}}(x) = \sum_{l}^{n} x_l \text{R}T \log(\gamma_l) = \sum_{i=1}^{n-1} \sum_{j>i}^{n} \Phi_i \Phi_j \frac{2 \sum_{l=1}^{n} \alpha_l x_l}{\alpha_i + \alpha_j} W_{ij} \tag{5}$$

The asymmetry of the excess Gibbs free energy function is controlled by the ratio of the different α values, which describe the properties of the end-members in the mixture and have been primarily related to their relative volumes in the mixture, although these parameters may be adjusted to fit experimental constraints (Holland and Powell, 2003). There are therefore $n-1$ independent α parameters and one of them may be set to unity (Holland and Powell, 2003). In a binary $i-j$ solution where $\alpha_i = \alpha_j$, the model is symmetric and the expression of $\overline{G}^{\text{xs}}_{\text{m}}(x)$ reduces to the sub-regular symmetric model where $\overline{G}^{\text{xs}}_{\text{m}}(x) = W_{ij} x_i x_j$.

The ASF model assumes that neither α_i nor W_{ij} vary with the composition of the solution although they may vary with pressure and temperature to satisfy the Gibbs-Duhem equation (see Spear, 1993). In the case of mixtures containing a solvus, α_i and W_{ij} can be evaluated solely from the compositions at binodal equilibrium and/or from the conditions of critical mixing, a separation of a two-phase system from a single-phase system. Details of the derivation of the parameters are given in Appendix B where the equations have been obtained in a manner similar to the derivation of De Capitani and Peters (1982) for the subregular model. It is noteworthy that in this case the chemical potentials of the end-members at standard state are not required to calculate compositions along solution binaries; it is thus possible to construct phase diagrams of binary solutions from the activity model alone, which can therefore be used with any database. Uncertainties on the activity-composition model may then be estimated independently from the uncertainties on the thermodynamic properties of the end-members.

Evans and Powell (2006, 2007) proposed parameterizations using DH-ASF in several binary and ternary systems, including H_2O-CO_2-NaCl, at temperatures greater than 400°C, where mixing parameters are either constant, linear functions of temperature, or proportional to the volume of water. Such simple models do not express activity-composition data adequately at lower pressures and temperatures, such as in the range of the two-phase H_2O-CO_2 domain (Fig. 1).

4. BINARY MIXTURES OF H_2O AND CO_2

The phase diagram controlling the solubilities of CO_2 and H_2O in the aqueous and CO_2-rich phases can be modeled with two components, for which we use the end-members H_2O and CO_2. Supplementary components such as carbonate species in the aqueous solutions are not required to calculate solubilities.

For aqueous species, we use the EOS of Holland and Powell (1998), modified from Holland and Powell (1990) to incorporate the density model of Anderson et al. (1991). This EOS is selected as a simple tool to estimate the thermodynamic properties of aqueous species at standard state over a large range of pressures and temperatures. We use the EOS for water given in the 2009 revised release of the International Association for the Properties of Water and Steam (IAPWS, available at http://www.iapws.org) and the Sterner and Pitzer (1994) EOS for CO_2 to calculate their respective densities, volumes and fugacities. The other routines for calculation of fugacities investigated during our study are not appropriate for the pressure and temperature range of interest: the CORK EOS (Holland and Powell, 1991) have not been constrained at temperatures lower than 100°C for either water or carbon dioxide, and the EOS derived by Pitzer and Sterner (1994), currently used in THERMOCALC, fails to reproduce the density of water accurately

at temperatures less than 130°C with a maximum density at about 45°C at all pressures less than 1kb rather than at 4°C at 1 bar. We also use the equations given by the IAPWS in their 1997 release to calculate the dielectric constant of water. The thermodynamic properties of the end-members used in this study are taken from the THERMOCALC database (Powell et al., 1998; Holland and Powell, 1998, 2003, 2011).

4.1. Application to the H_2O-CO_2 system

Although the H_2O-CO_2 system has been extensively studied and different parameterizations are available for calculating CO_2 solubility in water or brines, there is currently no activity-composition model which encompasses both low pressures and temperatures and high-grade metamorphic conditions. The very simple model of Holland and Powell (2003) where $W_{\mathrm{H_2O\text{-}CO_2}} = 10.5\frac{V_{\mathrm{CO_2}}+V_{\mathrm{H_2O}}}{V_{\mathrm{CO_2}}.V_{\mathrm{H_2O}}}$, $\alpha_{\mathrm{CO_2}} = V_{\mathrm{CO_2}}$ and $\alpha_{\mathrm{H_2O}} = V_{\mathrm{H_2O}}$ is based on the high pressure and temperature experiments by Aranovich and Newton (1999) and gives a satisfactory fit to the experimental data at pressures greater than 5 kbars but deviates from other experimental constraints at lower pressures (Fig. 1). The models developed by Spycher et al. (2003); García et al. (2006); Ji et al. (2005); Ji and Zhu (2012) or Duan and co-workers (Duan et al., 1992, 1995, 1996, 2000, 2003, 2006, 2008; Duan and Sun, 2003; Duan and Li, 2008; Duan and Zhang, 2006; Hu et al., 2007; Li and Duan, 2007; Mao and Duan, 2009) allow calculation of the solubility of CO_2 and densities of mixtures at various pressures and temperatures. Akinfiev and Diamond (2010) have proposed a thermodynamic model from a compilation and critical analysis of experimental results in the system H_2O-CO_2-NaCl reproducing the solubility of CO_2 and NaCl. However, their model is restricted to a small pressure-temperature range (less than 100°C and 1 kbar). As shown earlier, the

models of Duan and Sun (2003) and Duan et al. (2006) rely on erroneous assumptions. The thermodynamic models of Duan et al. (1992); Spycher et al. (2003); Ji et al. (2005) and Ji and Zhu (2012) account for the composition of the gas phase, but these models are either poorly constrained at low pressures and temperatures (e.g. Duan et al., 1992, is valid at conditions $>$ 100°C-200 bars) or restricted to low temperatures ($<$100°C, Spycher et al., 2003) or low pressures ($<$600 bars, Ji et al., 2005; Ji and Zhu, 2012). None of the above models give uncertainties on their calculated parameters.

We use the ASF formalism, with α_{H_2O} set to 1 and $W_{H_2O\text{-}CO_2}$ and α_{CO_2} functions of pressure and temperature, to model the mutual solubilities of H_2O and CO_2 up to temperatures of 370°C and pressures of 3500 bars. Figure 2a-c show the values of $W_{H_2O\text{-}CO_2}$ and α_{CO_2} as a function of pressure and temperature calculated for experimental results where both the amount of CO_2 in the aqueous phase and the amount of water in the CO_2-rich phase are measured. To do this, the experimental data gathered by Spycher et al. (2003) at temperatures lower than 110°C and the results of Todheide and Franck (1963) ranging from 50°C to 350°C and from 200 to 3500 bar have been used assuming binodal equilibrium. We have also used the results of Sterner and Bodnar (1991) and Mather and Franck (1992) who investigated the discrepancy between the measurements of Todheide and Franck (1963) and that of Takenouchi and Kennedy (1964), who report a solubility of water in the CO_2-rich phase about 20% higher at 1kb and 200°C, as noted by Joyce and Holloway (1993). Sterner and Bodnar (1991) and Mather and Franck (1992) found agreement with Todheide and Franck (1963) and therefore, we discarded the results of Takenouchi and Kennedy (1964) obtained at temperatures greater than 110°C. The CO_2 solubilities measured by Takenouchi and Kennedy (1964) and

Takenouchi and Kennedy (1965) also differ from Todheide and Franck (1963), especially at pressures below 600 bars and temperatures above 200°C, whereas the results of Todheide and Franck (1963) are generally higher. The results of Takenouchi and Kennedy (1965) have therefore not been used to parameterize the model in H_2O-CO_2, but their measurements in H_2O-CO_2-NaCl were used as described below.

When not given in the original publication, experimental uncertainties have been estimated as $\pm 3\%$ of the measured CO_2 content in the water-rich phase and $\pm 1\%$ of the measured CO_2 content in the CO_2-rich phase, in line with the commonly reported uncertainties. Although reported compositions vary, there is a general agreement between Todheide and Franck (1963) and Takenouchi and Kennedy (1964) on the pressure and temperature conditions of critical mixing. To the previously described experimental results, we have added the measurements of CO_2 solubility reviewed and selected by Diamond and Akinfiev (2003) in the range 0-100°C and 1-1000 bars (namely: Sander, 1912; Hähnel, 1920; Kritschewsky et al., 1935; Zelvinskii, 1937; Wiebe and Gaddy, 1939, 1940; Bartholomé and Friz, 1956; Vilcu and Gainar, 1967; Matous et al., 1969; Stewart and Munjal, 1970; Malinin and Saveleva, 1972; Malinin and Kurovskaya, 1975; Zawisza and Malesinska, 1981; Gillespie and Wilson, 1982; Müller et al., 1988; Namiot, 1991; King et al., 1992; Teng et al., 1997; Bamberger et al., 2000; Yang et al., 2000; Servio and Englezos, 2001; Anderson, 2002). When these measurements do not include the composition of the gas phase, it has been evaluated for each experimental point from a version of the model with $W_{\mathrm{H_2O\text{-}CO_2}}$ and $\alpha_{\mathrm{CO_2}}$ derived from the dataset without these measurements. The estimated gas composition was given a very large uncertainty (100% of the water content) to ensure that

the uncertainty on $W_{\mathrm{H_2O\text{-}CO_2}}$ and $\alpha_{\mathrm{CO_2}}$ is effectively constrained by the measured aqueous composition, giving negligible weight to the estimated gas compositions.

As shown on figure 2, neither $W_{\mathrm{H_2O\text{-}CO_2}}$ nor $\alpha_{\mathrm{CO_2}}$ are linear functions of pressure and temperature, and they vary rapidly close to the phase transitions of the end-members. At conditions below the critical point of water, the solvus closes on the composition of water. In this case the value of $\alpha_{\mathrm{CO_2}}$ tends towards $+\infty$ and it is not possible to use ASF at the exact conditions of boiling water. This feature is nonetheless a strong constraint on the shape of the $\alpha_{\mathrm{CO_2}} = f(P,T)$ surface (Fig. 2c). The scale of the $\alpha_{\mathrm{CO_2}}$ diagram on figure 2c has been chosen to exclude the very high values from experimental results close to the boiling curve of water. Interestingly, the quantity $W_{\mathrm{H_2O\text{-}CO_2}}/\mathrm{R}T$ is remarkably linear over the range of pressure and temperature where CO_2 is liquid or supercritical. $\alpha_{\mathrm{CO_2}}$ is similarly nearly linear with pressure and temperature at pressures greater than 500 bars. The data scatter close to the following least squares fits to linear relationships:

$$W_{\mathrm{H_2O\text{-}CO_2}}/\mathrm{R}T = 5.41 - 0.276P - 1.07T * 10^{-2} \quad (6)$$

$$\alpha_{\mathrm{CO_2}} = 0.742 - 0.0974P + 3.32T * 10^{-3} \quad (7)$$

with correlation coefficients (r^2) of 0.97 for $W_{\mathrm{H_2O\text{-}CO_2}}/\mathrm{R}T$ and of 0.96 for $\alpha_{\mathrm{CO_2}}$. However, the approximate linear relationships break down at lower pressures in the vicinities of the boiling curve of water and the critical point of CO_2. To capture the precision of the experimental results, we have parameterized $W_{\mathrm{H_2O\text{-}CO_2}}/\mathrm{R}T$ and $\alpha_{\mathrm{CO_2}}$ with polynomial functions of the density of the co-solvents H_2O and CO_2. This accounts for the abrupt changes in the parameters in pressure-temperature space (Fig. 2d). $W_{\mathrm{H_2O\text{-}CO_2}}/\mathrm{R}T$ and $\alpha_{\mathrm{CO_2}}$ have been modeled as ratios of polyno-

mials of the form N_i/D_i, with:

$$N_i = 1 + k_{i,1}.a + k_{i,2}.a^2 + k_{i,3}.a^3 + k_{i,4}.a^4 + k_{i,5}.b + k_{i,6}.b^2 + k_{i,7}.b^3 + k_{i,8}.b^4 + k_{i,9}.a.b + k_{i,10}.a^2.b^2 \quad (8)$$

$$D_i = k_{i,11} + k_{i,12}.a + k_{i,13}.a^2 + k_{i,14}.a^3 + k_{i,15}.a^4 + k_{i,16}.b + k_{i,17}.b^2 + k_{i,18}.b^3 + k_{i,19}.b^4 + k_{i,20}.a.b + k_{i,21}.a^2.b^2 \quad (9)$$

where i represents either $W_{\mathrm{H_2O\text{-}CO_2}}/\mathrm{R}T$ or $\alpha_{\mathrm{CO_2}}$, a is the density of pure H_2O and b is that of CO_2. The use of ratios of polynomial equations has been chosen to accommodate trends towards infinity. Values for $k_{W_{\mathrm{H_2O\text{-}CO_2}}/\mathrm{R}T}$ and $k_{\alpha_{\mathrm{CO_2}}}$ are given in tables D1 and D2 of Appendix D.

Simpler expressions than equations 8 and 9 would be preferable but the approach used here gives accurate results for both critical mixing and reciprocal solubilities of CO_2 and H_2O over the whole pressure-temperature range.

The adjustable parameters were calibrated by minimization of the reduced χ^2_ν (defined as $\chi^2_\nu = \frac{1}{\nu}\sum_{j=1}^{n}\frac{(v_{Mj}-v_{Cj})^2}{\sigma_j^2}$ where v_{Mj} and v_{Cj} are measured and calculated values for experiment j and ν the degree of freedom) using the Levenberg-Marquardt algorithm (Levenberg, 1944; Marquardt, 1963). To reduce the number of adjustable parameters, an F test (as defined by Bevington and Robinson, 2002) has been run where parameters were successively zeroed until the quality of the fit was significantly lowered.

The fits to the experimental results and calculated phase diagrams are illustrated in figures 3 and 4. At pressures lower than the critical point of water, the solvus closes on the boiling curve of water with a CO_2-free composition (i.e. on the y axis of Fig. 3a, 3b and 3c). At pressures higher than the critical point of water, the temperature of critical mixing decreases with increasing pressure (Fig. 1

and 3d). CO_2 solubility is also well calculated at low pressures and temperatures, where the sharp difference of increase in CO_2 solubility with pressure along the boiling curve of CO_2 is well reproduced (figure 4).

Uncertainties on the adjustable parameters of equations 8 to 9 have been estimated with the help of a Monte-Carlo simulation. The system was calculated 1000 times by allowing the compositions of the experimental results used to calculate $W_{\mathrm{H_2O\text{-}CO_2}}$ and $\alpha_{\mathrm{CO_2}}$ to vary within the limits of their uncertainty (or defined by the misfit of the model to the data when this was greater than experimental uncertainty). The resulting covariance matrices are given in tables D1 and D2 of appendix D and allow the uncertainty on the compositions to be recovered from the uncertainty on $\overline{G}_{\mathrm{m}}^{\mathrm{xs}}(x)$ with the usual error propagation equation (e.g. Bevington and Robinson, 2002, their equation 3.13).

The calculated parameters are strongly correlated due to the nature of the functions and the covariance terms can consequently not be neglected.

An indicative map of uncertainties in calculated CO_2 solubility is provided in figure 5. At pressures greater than 500 bars, experiments are generally reproduced within their uncertainties (of the order of 10% of the measured value at low temperatures). At low pressure and high temperature, the model can diverge from experimental values, especially in the vicinity of the boiling curve of water where CO_2 solubility is very small. Below the critical point of CO_2, the model reproduces the experiments less well at very low pressures where the CO_2 concentrations are very small.

4.2. Activities of water and carbon dioxide in saturated mixtures

Phase assemblages may be very sensitive to variations of the activity of water, in both low- and high-grade metamorphic rocks (Greenwood, 1967; Ferry, 1984;

406 Nicollet and Goncalves, 2005; Le Bayon et al., 2006; Vidal and Dubacq, 2009).
407 The dilution of water by addition of CO_2 in solution decreases the activity of water
408 (e.g., Santosh and Omori, 2008) and may consequently decrease the temperatures
409 of dehydration reactions.

410 Figure 6 illustrates the calculated activity of water (a_{H_2O}, Fig. 6a) and ac-
411 tivity coefficient of water (γ_{H_2O}, Fig. 6b) in a CO_2-saturated aqueous phase in
412 the pressure-temperature range where two phases coexist. At low pressure, a_{H_2O}
413 decreases with increasing pressure roughly parallel to the water vapor curve. At
414 pressures higher than 1kb, a_{H_2O} is more sensitive to temperature. a_{H_2O} remains
415 elevated even in the vicinity of the critical curve (dashed line on Fig. 6), because
416 the composition of the mixture tends to that of water along the boiling curve of
417 water; at pressures higher than the critical point of water, the positive deviation
418 from ideal gas behavior (γ_{H_2O} and $W_{H_2O\text{-}CO_2} > 0$) increases a_{H_2O} and compensates
419 for the dilution of water by CO_2: for example, at 270°C and 1 kbar, the water-rich
420 phase is a mixture of 18 mol. $\%$ of CO_2 and 82 mol. $\%$ of water but the water
421 activity is as high as 0.91.

422 Figure 6c and d present a_{CO_2} and γ_{CO_2} in the water-saturated CO_2-rich phase as
423 a function of pressure and temperature. γ_{CO_2} is significantly greater than one over
424 a large range of pressures and temperatures, especially close to the boiling curve of
425 water. At 1 bar, $\gamma_{CO_2} = 1.01$ at 50°C and $\gamma_{CO_2} = 1.07$ close to 100°C. Generally,
426 the calculated a_{CO_2} decreases with temperature but increases with pressure. Very
427 low a_{CO_2} is obtained at low pressure in the vicinity of the boiling curve of water,
428 and a_{CO_2} becomes gradually less sensitive to pressure with increasing pressure.

4.3. Density calculations for H_2O-CO_2 mixtures

Densities calculated with the present model show a good accuracy at conditions greater than the boiling curves of CO_2 and water, at both low and high CO_2 concentrations. As shown in table 3, the densities of the water phase saturated in CO_2 measured by Teng et al. (1997) at temperatures lower than 20°C are reproduced within 4‰ at pressures greater than 150bars. The measurements of Hnedkovský et al. (1996), carried out below CO_2 saturation ($\sim$0.15mol/kgH_2O), are reproduced well away from the boiling curve of water but there is a significant deviation with the calculated values ($>$10‰) at low water density. In the gaseous field of CO_2, density calculations do not give satisfactory results either. This is attributed to the use of H_2O and CO_2 as end-members in the calculations. In the gaseous field of CO_2, the volume of the CO_2 end-member is very sensitive to pressure with the result that the calculated density shows a comparable sensitivity. Consequently, even if errors on the activity model are small, errors on the calculated densities are large at very low densities. Similarly, the experimental results at 59°C of Li et al. (2004) are well reproduced above 100 bars after recalibration for systematic deviations (see Duan et al., 2008). A map of densities calculated over the range 0.1-3kb and 50-370°C is presented in figure 7.

5. BINARY MIXTURES: H_2O-NaCl

The H_2O-NaCl system has been extensively studied for decades (see Driesner and Heinrich, 2007, for a review). The solubility of halite is known to be more sensitive to temperature than to pressure (e.g, Bodnar, 1994), and NaCl dissociates into several species in solution (see Oelkers and Helgeson, 1993; Sharygin et al., 2002) because of the pairing of Na^+ and Cl^- ions. The neutral aqueous sodium

chloride species $NaCl^0$ is thought to dominate the associated NaCl species in solution over a large range of pressure, temperature and composition (Sharygin et al., 2002), but it has been proposed that polynuclear species (Na_2Cl^+, $NaCl_2^-$, etc) also occur (e.g. Sherman and Collings, 2002). The derivation of thermodynamic properties of such polynuclear species is beyond the scope of this study and all associated species are here considered as $NaCl^0$.

5.1. DH-ASF formalism and the Anderson density model

With the DH-ASF model, Na^+ and Cl^- ions are represented by a single end-member $(NaCl\pm)_{1/2}$, and the reaction describing halite $NaCl_{(cr)}$ dissolution is:

$$NaCl_{(cr)} \leftrightarrow 2(NaCl\pm)_{1/2} \tag{10}$$

The pairing of Na^+ and Cl^- into $NaCl^0$ (or its dissociation) is calculated with the reaction:

$$2(NaCl\pm)_{1/2} \leftrightarrow NaCl^0 \tag{11}$$

The total number of moles of dissolved NaCl is thus equal to $(1/2)(NaCl\pm)_{1/2} + NaCl^0$. The subscript 1/2 will be dropped from this point onwards for convenience.

The thermodynamic properties of $NaCl\pm$ have been calculated from that of Na^+ and Cl^- from Helgeson et al. (1981) as used in the THERMOCALC database (Holland and Powell, 2011). It has been found necessary to recalculate the heat capacity terms (Cp^0 and b_{Cp}, see Holland and Powell, 1998) of $NaCl\pm$ by fitting them to the measurements reported in Pitzer et al. (1984) as shown in figure 8a. Obtained values are $Cp^0 = -0.0417156$ kJ/K and $b_{Cp} = -20.8763 * 10^5$ kJ.K^2. The volumes calculated at infinite dilution of $NaCl\pm$ using the calculated heat

capacity via the modified Anderson density model EOS fit the volumes inferred from experimental results (Fig. 8b). However, volumes obtained above the critical temperature of water show a non-reasonable pressure dependency at pressures lower than about 1 kbar, as illustrated in figure 8c. This has been identified as originating from the use of the ratio $\rho_{H_2O}/\rho^0_{H_2O}$ in the derivation of the chemical potential of Anderson et al. (1991, Fig. 8d), where $\rho^0_{H_2O}$ is the density of water at standard pressure and temperature and ρ_{H_2O} is the density of water at the considered pressure-temperature. It is therefore not possible to calculate accurate densities for aqueous fluids in the range of approximately 370-550°C at pressures below about 1 kbar with this EOS, which nevertheless shows good accuracy in many geologically relevant thermal gradients.

The thermodynamic properties of the end-member $NaCl^0$ were based on those of molten halite (Evans and Powell, 2006).

The uncertainties on the formation enthalpy ΔH^0_f, as reported by Holland and Powell (2011) for halite, $NaCl\pm$ and $NaCl^0$, are of similar relative magnitude at $\sim 0.5‰$ of their ΔH^0_f. This corresponds to a precision of $\sim \pm 0.1$ molal for the calculation of the solubility of halite at STP.

5.2. Parameterization of the activity model

The relative amounts of $NaCl\pm$ and $NaCl^0$ vary non-linearly as a function of the concentration of aqueous sodium chloride and may be described by five parameters between the end-members in equations 10 and 11: $W_{NaCl\pm\text{-}H_2O}$, $W_{NaCl^0\text{-}H_2O}$, $W_{NaCl\pm\text{-}NaCl^0}$, $\alpha_{NaCl\pm}$ and α_{NaCl^0}. It is assumed that $W_{NaCl\pm\text{-}NaCl^0} = 0$ as this term has little effect on the calculated equilibria.

Solubility, density and conductivity measurements were used to parameterize the activity model. Selected solubility experiments range from 15 to 650°C and

from 1 bar to 10 kbar (table 2). The data are mostly consistent, with the exception of the high pressure measurements of Sawamura et al. (2007) who report solubility values for halite higher by up to 2% than the measured values at 2-3kb and 25°C of Adams (1931) (figure 9).

Measurements of the conductance of NaCl solutions are used to estimate the degree of dissociation of $NaCl^0$ into Na^+ and Cl^- (eq. 11) via:

$$x_{\mathrm{NaCl}\pm} = \Lambda\epsilon/\Lambda e \tag{12}$$

where $x_{\mathrm{NaCl}\pm}$ is the fraction of NaCl dissolved as NaCl$\pm$, $\Lambda\epsilon$ is the experimentally determined equivalent conductance and Λe is the equivalent conductance of a hypothetical completely dissociated NaCl solution of the same effective ionic strength (Oelkers and Helgeson, 1988). The procedure selected to calculate $\Lambda\epsilon/\Lambda e$ is described in Appendix C, and we used the measurements of Bianchi et al. (1989), Chambers et al. (1956) and Quist and Marshall (1968). At 25°C and 1 bar, the calculated $\Lambda\epsilon/\Lambda e$ indicate that, within uncertainties of the data, corrections and equations used, at least 95% of the aqueous NaCl is dissociated up to 5.35 molal, in agreement with Monica et al. (1984) but strikingly different from the results of Sherman and Collings (2002) whose molecular dynamic simulations predict about 50% of aqueous NaCl to be as $NaCl^0$ or larger polynuclear species at 6 molal. Only values of $x_{\mathrm{NaCl}\pm}$ estimated from conductance measurements have been used in this work. At constant molality, $\Lambda\epsilon/\Lambda e$ decreases with temperature and increases with pressure, as noted by Oelkers and Helgeson (1988) and shown in figure 11.

The calculated volume of the NaCl$\pm$ end-member at its hypothetical pure standard state depends on both 1) the thermodynamic properties of the usual hypothetical Na^+ and Cl^- 1 molal aqueous species derived from infinite dilution and 2) on

the interaction parameters $W_{\text{NaCl}\pm\text{-H}_2\text{O}}$ and $\alpha_{\text{NaCl}\pm}$ because they affect the chemical potential of the NaCl$\pm$ end-member within the DH-ASF framework. NaCl being largely dissociated under 100°C, NaCl^0 has little effect on the Gibbs energy of the mixture and on its pressure dependency. Consequently, the pressure dependency of $W_{\text{NaCl}\pm-\text{H}_2\text{O}}$ and $\alpha_{\text{NaCl}\pm}$ are constrained mainly by the chosen density measurements (Surdo et al., 1982). The temperature dependency of these parameters has been estimated together with that of $W_{\text{NaCl}^0\text{-H}_2\text{O}}$ and $\alpha_{\text{NaCl}\pm}$ by fitting high-temperature solubility experiments (Fig. 9a) and calculated degree of association (Fig. 11a, equation C1).

The following expressions have been found to provide a good description of the system in the pressure-temperature range 1bar-10kbar and 20-650°C, as shown in figures 10, 9 and 11:

$$W_{\text{NaCl}^0\text{-H}_2\text{O}} = C_1 + C_2.P + C_3.T + C_4.P^2 \tag{13}$$

$$\alpha_{\text{NaCl}^0} = C_5 + C_6.P + C_7.T \tag{14}$$

$$W_{\text{NaCl}\pm\text{-H}_2\text{O}} = C_8 + C_9.T_{400} + C_{10}.T_{400}^2 + C_{11}.P + C_{12}.P^2 \tag{15}$$

$$\alpha_{\text{NaCl}\pm} = C_{13} + C_{14}.T + (C_{15}. + C_{16}.T)P \tag{16}$$

where T_{400} is temperature below 400K such as $W_{\text{NaCl}\pm\text{-H}_2\text{O}}$ is independent of temperature above 400K. Values for the C constants are given in Table D3 of Appendix D.

5.3. Results and error propagation

The correlation between the calculated and measured solubilities is good (Fig. 9). This model gives a better fit to high-temperatures data than the model of Mao and Duan (2008, dotted line on Fig. 9). The obtained parameters agree well with

the results of Aranovich and Newton (1996) who found that the system is very close to ideality around 2 kbar and 500°C ($W_{\mathrm{NaCl^0-H_2O}} = 0.56$ kJ.mol^{-1}). Density measurements in the aqueous phase are very well reproduced below the critical point of water and are in close agreement with the model of Driesner (2007). At higher temperatures, our model diverts from the model of Driesner (2007) (Fig. 10b and c) for pressures around 1 kbar and below. The calulated dissociation of $NaCl^0$ presented in figure 11a is consistent with the measurements of Quist and Marshall (1968) as it shows the same variations with pressure and temperature but appears systematically offset by a few percents, which could not be solved without allowing unrealistically low values for $\alpha_{\mathrm{NaCl^0}}$. The uncertainties associated with the original values of $\Lambda\epsilon$ and Λ_0 reported by Quist and Marshall (1968) cumulate to a minimal uncertainty of about 10% of the given $x_{\mathrm{NaCl}\pm}$ value at water densities below 0.5 and between 4 and 10% at higher densities. Because 1) uncertainties associated with the use of equations C2 and C3 are unknown, 2) the possible role of large polynuclear species, although unclear (Sharygin et al., 2002), can not be ruled out and 3) the low ratio of NaCl$\pm$ to $NaCl^0$ makes $W_{\mathrm{NaCl}\pm-\mathrm{H_2O}}$ poorly constrained at temperatures greater than 500°C, we have adopted an expression for the activity model in which $W_{\mathrm{NaCl}\pm-\mathrm{H_2O}}$ is independent of temperature above 400 °C and $\alpha_{\mathrm{NaCl}\pm}$ varies linearly with pressure but with a temperature-dependent slope.

Error propagation has been performed by a Monte-Carlo simulation where the system has been refitted 100 times, by varying the original experimental results within the misfit of the model to the data and the enthalpy of formation of the aqueous species within their uncertainties. To simplify the propagation of errors on the activity model, the correlation of uncertainties associated with the enthalpy

of formation of the aqueous species given in the THERMOCALC database has been neglected. The covariance matrix associated with C_1 to C_{16} is given in Table D3.

6. THE H_2O-CO_2-NaCl SYSTEM

The solubility of CO_2 in the water phase decreases with increasing salinity of the aqueous phase (termed salting-out, e.g.: Markham and Kobe, 1941; Drummond, 1981; Nighswander et al., 1989; Rumpf et al., 1994). The combination of the subsystems H_2O-CO_2 and H_2O-NaCl needs two additional interaction parameters to describe H_2O-CO_2-NaCl: $W_{CO_2\text{-}NaCl^0}$ and $W_{CO_2\text{-}NaCl\pm}$. Salting-out implies positive values for these parameters. The magnitudes of $W_{CO_2\text{-}NaCl^0}$ and $W_{CO_2\text{-}NaCl\pm}$ are expected to be high given that NaCl is barely incorporated in the CO_2-rich phase in the absence of water, even at high pressure and temperature: the measurements of Zakirov et al. (2007) indicate a NaCl mole fraction of $30 * 10^{-7}$ in the CO_2 phase at 670 bars and 400°C. In H_2O-CO_2-NaCl, taking the CO_2-rich phase to be free of NaCl is an acceptable approximation up to at least 300°C (e.g. Hu et al., 2007, and references herein). With this assumption, the solubility of CO_2 in the aqueous NaCl solution can be calculated by minimizing the Gibbs free energy of the system, composed of a water-saturated CO_2-rich phase and of the aqueous phase at fixed NaCl content. The relative proportions of $NaCl^0$ and $NaCl\pm$ are calculated by solving equation 11 with the appropriate interaction parameters (eq. 8,9,13,14,15,16).

As pointed out by Hu et al. (2007), there is currently no accurate model to predict the solubility of CO_2 in NaCl brines at temperatures greater than about 60°C, mainly due to the scarcity of experimental results at these pressures and

temperatures. In particular, the measurements of Takenouchi and Kennedy (1965) (ranging up to 1400 bars and 450°C) are not in agreement with other experiments at pressures below 300 bars, some of which we used here (Ellis and Golding, 1963; Drummond, 1981; Nighswander et al., 1989; Rumpf et al., 1994; Kiepe et al., 2002). The measurements of Takenouchi and Kennedy (1965) at zero NaCl content are also inconsistent (by up to 15%, see Fig. 12b) with the measurements of Todheide and Franck (1963) which we used to constrain the H_2O-CO_2 activity model. However, all the data of Takenouchi and Kennedy (1965) at $x_{NaCl} > 0$ have been kept in our regression as they are the major source of measurements available above 500 bars.

It was assumed that $W_{\text{CO}_2\text{-NaCl}^0} = W_{\text{CO}_2\text{-NaCl}^\pm}$ because the quality of the fit to the data is not statistically sensitive to the ratio $W_{\text{CO}_2\text{-NaCl}^0}/W_{\text{CO}_2\text{-NaCl}^\pm}$. $W_{\text{CO}_2\text{-NaCl}^0}$ and $W_{\text{CO}_2\text{-NaCl}^\pm}$ may then be estimated from solubility experiments independently of the thermodynamic properties of pure H_2O and CO_2 and of their uncertainties. However obtained values depend on the activity models in H_2O-CO_2 and H_2O-NaCl. As observed in the H_2O-CO_2 system, the quantity $W_{\text{CO}_2\text{-NaCl}^\pm}/(\text{R}T)$ shows smoother variations in pressure-temperature space than $W_{\text{CO}_2\text{-NaCl}^\pm}$, although both values increase strongly with pressure especially under 100 bars. For this reason, $W_{\text{CO}_2\text{-NaCl}^\pm}$ has been parameterized as a function of the natural logarithm of pressure:

$$W_{\text{CO}_2\text{-NaCl}^\pm}/(\text{R}T) = D_1 + D_2 \ln P + D_3.T + D_4 T \ln P + D_5 (\ln P)^2 \qquad (17)$$

where pressure is in bar and temperature in Kelvin. Values for D_1 to D_5 are given in table D4.

Figure 12 illustrates the calculated salting-out effect and presents the quality of the fit of the model to some of the experimental data. Error propagation has

been carried out as in the previous systems by a Monte-Carlo simulation where experimental uncertainties are estimated from the misfit of the model with the experimental results. The covariance matrix for D_1 to D_5 is given together with their values in table D4. The correlation of uncertainties between parameters regressed for the activity models in the subsystems H_2O-CO_2 and H_2O-NaCl and this system has been neglected because uncertainties from experiments and the models in the subsystems are smaller than in H_2O-CO_2-NaCl.

7. DISCUSSION

7.1. Accuracy and advantages of the method

The method used here to parameterize the H_2O-CO_2 activity model is independent of the thermodynamic properties of the co-solvents and successfully reproduces the experimentally-derived phase diagram over the whole two-phase domain. The solubility of CO_2 is also calculated well by other models, in particular Duan et al. (2006, figure 3), although it has been shown that this model does not provide a correct derivation of the chemical potential of CO_2. The models of Spycher et al. (2003) and Akinfiev and Diamond (2010) give excellent fit to the aqueous phase experimental results at temperatures below 100°C. The principal advantages of the model presented here are 1) the facility to model the CO_2-rich phase, 2) the wider pressure-temperature range of applicability, and 3) the ease of error propagation provided by separate uncertainties for the activity model and the end-members.

In the H_2O-NaCl system, the DH-ASF activity model reproduces the experimental data on the solubility of halite over a wide range of pressures and temperatures. Here, the form of the pressure and temperature dependency of the activity

parameters have been fitted to solubilities, densities and conductivity measurements, giving reasonable values for $\alpha_{\mathrm{NaCl}\pm}$ and α_{NaCl^0} whose variations over 10 kb and 600 °C do not exceed 0.4 and 0.8 α unit, respectively. Their pressure derivatives, implied by density measurements, are particularly small (at a maximum magnitude of 5.10^{-3} kbar^{-1}) and of opposite signs, making it difficult to link them to variations of the properties of the solvent. The pressure dependencies of $W_{\mathrm{NaCl}^0\text{-}\mathrm{H_2O}}$ and $W_{\mathrm{NaCl}\pm\text{-}\mathrm{H_2O}}$ are similarly small, which is imposed by the insensitivity of halite solubility to pressure.

Results in H_2O - CO_2 - NaCl are compared in figure 12 to the model of Duan and Sun (2003) on which the model of Duan and Zhang (2006) is based. At pressures and temperatures under 100°C and 100 bars, our model gives results very similar to Duan and Sun (2003). At higher pressures and temperatures, the model of Duan and Sun (2003) gives a better fit to the data of Takenouchi and Kennedy (1965), which are often lower than expected from the measurements of Todheide and Franck (1963), well reproduced by our model. For this reason, our model gives solubilities greater than the data of Takenouchi and Kennedy (1965) and the model of Duan and Sun (2003) at pressures and temperatures where Todheide and Franck (1963) and Takenouchi and Kennedy (1965) are not in agreement (Fig. 12). However, the curvature of the CO_2 solubility is quite similar for both models at NaCl concentrations below 3 molal. The model presented in this study has been fitted with essentially the same dataset as in Duan and Sun (2003) for the system H_2O - CO_2 - NaCl, where high-pressure-temperature measurements are restricted below about 4 molal NaCl. However our model gives more plausible extrapolation to higher concentrations than Duan and Sun (2003, e.g. Fig. 12b), where their approach predicts an increase of the CO_2 solubility with increasing NaCl

molality, which is not supported by any data to our knowledge. Our model, whose parameters do not depend on concentration, predicts a continuous decrease in CO_2 solubility with increasing salinity over the entire pressure-temperature range and up to 10 molal NaCl.

7.2. Range of applicability

The pressure-temperature range of the activity model proposed for H_2O-CO_2 is limited to the two-phase domain. Equations B11, B13, B18 and B19 provide a simple and accurate parameterization of the system H_2O-CO_2 but only over pressure-temperature conditions where two phases coexist. The parameterization can not be extrapolated to the one-phase domain below the critical point of water (Fig. 1): although a_{CO_2}/α_{H_2O} tends towards infinity near the boiling curve of water, there is no simple relation between a_{CO_2} and V_{CO_2}/V_{H_2O}. Extrapolation of the model towards low temperatures or high pressures in the liquid field of CO_2 is speculative as there are few experimental results to constrain its pressure-temperature dependency. It has been noted in section 2.2 and figure 2b that away from the boiling curve of water and critical point of carbon dioxide, both $W_{H_2O\text{-}CO_2}/RT$ and a_{CO_2} show a fairly linear behavior. However, it is probable that the observed trends can be extrapolated over a larger range of pressures and temperatures. Models (e.g. Johnson, 1991; Holland and Powell, 2003, Fig. 1) suggest that the critical temperature increases significantly at pressure greater than 3.5 kb, implying that $W_{H_2O\text{-}CO_2}$ increases with increasing pressure, opposite to the trend observed below 3500 bars. As shown in figure 13, the departures at higher temperatures from the model of Holland and Powell (2003), calibrated in the one-phase domain, imply that the decrease of $W_{H_2O\text{-}CO_2}/RT$ with temperature (Fig. 2) is likely to be reversed in the one-phase domain.

There are therefore abrupt changes in the parameters describing the thermodynamic properties of the mixture both along the critical mixing curve (Fig. 13) and along along the phase transitions of the end-members (e.g. steps in $W_{\mathrm{H_2O\text{-}CO_2}}$ along the boiling curve of CO_2, Fig. 2d; $\alpha_{\mathrm{CO_2}} \rightarrow \infty$ along the boiling curve of water, Fig. 2c).

For these reasons our model (equations 8-9) should not be extrapolated to the one-phase region (Fig. 1) where the model of Holland and Powell (2003) is appropriate. The critical curve which delimits the domain of applicability can be closely approximated from the critical point of water up to 3000 bars by:

$$T_{\mathrm{C}} = q_1 + q_2.P + q_3.P^2 + q_4.\log(P) \tag{18}$$

where q_1 to q_4 are constants obtained by regression analysis ($R^2 = 0.993$) of the data of Todheide and Franck (1963) and Takenouchi and Kennedy (1964): $q_1 = 195.3, q_2 = 90.36, q_3 = -8.945, q_4 = -107.9$.

8. CONCLUSIONS

The model presented here is unique in that it replicates available data for mixed phase, salt-rich, mixed-solvent fluids close to the critical end point, allows realistic propagation of uncertainties, simulates dissociation of ionic solutes such as NaCl, can be extended readily to more complex systems as calibration data becomes available, is compatible with existing thermodynamic databases and software, and is based, as far as possible, on physically realistic expressions with a minimum reliance on empirical expressions such as power-law series.

It is possible to calculate accurate phase diagrams for CO_2-H_2O mixtures in the two-phase domain with macroscopic interaction parameters and associated

uncertainties independently of the standard state chemical potentials of water and carbon dioxide. Such calculations are straightforward, fast, lead to a unique result and do not depend on the quality of the chosen thermodynamic database. They can be implemented in Gibbs energy minimization routines (e.g. Connolly, 2009; De Capitani and Petrakakis, 2010).

The interaction parameters $W_{\mathrm{H_2O\text{-}CO_2}}$ and $a_{\mathrm{CO_2}}$ calculated from experimental results show non-linear variations with pressure and temperature, reflecting significant changes of solubilities and volumes for example along the vapor-liquid transition curves of water and carbon dioxide. This contrasts with the description of the higher temperature-pressure conditions applicable to metamorphic petrology where the linear relation $W_G = W_H - T * W_S + P * W_V$ holds for the many systems described by the subregular model or the ASF formalism. As a consequence, it is not possible to extrapolate mixing parameters in the one-phase domain from compositions at equilibrium in the two-phase domain in the H_2O-CO_2 system.

An activity model in the H_2O-NaCl system was derived with a similar thermodynamic formalism, DH-ASF (Evans and Powell, 2006), which uses hypothetical end-members with unit activity at standard state for aqueous species. This model requires a small number of concentration-independent interaction parameters, which we parameterized up to 10kbars and 650°C as a function of pressure and temperature using density, conductivity and solubility measurements.

The activity models in H_2O-CO_2 and H_2O-NaCl were combined to propose an activity model in the H_2O-CO_2-NaCl system where the decrease of CO_2 solubility with salinity is explained by positive values for W parameters between dissolved NaCl and CO_2. It is shown that our approach extrapolates to high salin-

737 ities without diverging from the expected decrease in CO_2 solubility, in contrast
738 with the model of Duan and Sun (2003). The fit to the experimental data is good
739 and uncertainties on all parameters of the activity model are estimated.

740 Addition of activity models for aqueous species and gases to the THERMO-
741 CALC database with the DH-ASF formalism is in progress (e.g. Evans et al.,
742 2010).

743 9. ACKNOWLEDGMENTS

744 This work was supported by the EU Marie Curie GRASP RTN and the NERC
745 through the CRIUS consortium. We thank Éric Lewin for help in regression anal-
746 ysis and Roger Powell, Tim Holland, Niko Kampman, Olivier Namur, Oli Shorttle
747 and Ed Tipper for helpful discussions. Jacques Schott (A.E.) and three anonymous
748 reviewers are thanked for their numerous comments and suggestions on previous
749 versions of the manuscript.

APPENDIX A

The formalism of DH-ASF allows for the description of the Debye-Hückel effect arising from long-range interactions at low concentrations and of short-range forces at high concentrations. The evolution of the chemical potential of the aqueous species A is illustrated in figure A1. The standard state μ_A^0 is defined in the A end-member at $x_A = 1$. $\mu^0 A$ is augmented from the ideal line at $x = 1$ by the sum of all non-ideal contributions: long-range electrostatic forces at low concentrations where μ is below the ideal mixing line and short-range interactions at higher concentrations. At very low concentrations of A, μ_A nears the ideal line (dashed on Fig. A1). With increased concentration of A, μ_A evolves to $\mu_A < mu_{ideal}$ (e.g. at $x = x_1$) due to the Debye-Hückel effect. The effect of long-range interactions has been limited in the modeling to a maximum of 0.1 molal by Evans and Powell (2006). For solutions more concentrated than 0.1 molal, the activities of the end-members in solution are described by the short-range interaction parameters of the ASF model. On figure A1, these constrain the part of the diagram where μ_A is greater than the line of ideal mixing (e.g. at $x = x_2$).

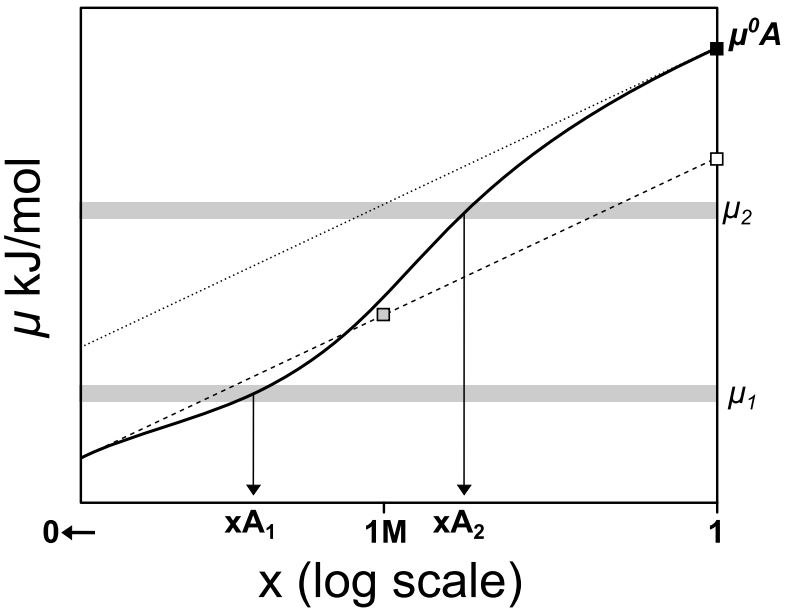

Figure A1: Schematic illustration of the relationship between chemical potential and concentration in the DH-ASF formalism for the aqueous species A. The solid line indicate measured chemical potential. The broken line shows the chemical potential of an ideal solution referenced to infinite dilution for A. The usual 1M standard state is indicated with a gray symbol, and its equivalent projected at x=1 along the ideal mixing line shown with an open symbol. The dotted line shows the chemical potential for an ideal solution referenced to a hypothetical ideal solution at $x = 1$. Modified after Evans and Powell (2006).

APPENDIX B

It is demonstrated here that if unmixing occurs in a binary $i-j$ solution, it is possible to calculate the values of the parameters W_{ij} and α_i/α_j from the compositions of the coexisting phases x_1 and x_2 at equilibrium, i.e. from the binodal solvus.

In a binary $i-j$ solution, where x is the proportion of the j end-member so that $\mathrm{x_i} = 1 - \mathrm{x}$, chemical potentials can be expressed as (e.g. Guggenheim, 1977):

$$\mu_i(x) = \overline{G}_{\mathrm{m}}(x) - x\frac{\delta \overline{G}_{\mathrm{m}}(x)}{\delta x} \tag{B1}$$

$$\mu_j(x) = \overline{G}_{\mathrm{m}}(x) + (1-x)\frac{\delta \overline{G}_{\mathrm{m}}(x)}{\delta x} \tag{B2}$$

where $\overline{G}_{\mathrm{m}}(x)$ is the molar Gibbs free energy of the mixture:

$$\begin{aligned}\overline{G}_{\mathrm{m}}(x) = (1-x)\mu_i^0 + x\mu_j^0 + \mathrm{R}T(1-x)\log(1-x) \\ +\mathrm{R}Tx\log(x) + \overline{G}_{\mathrm{m}}^{\mathrm{xs}}(x)\end{aligned} \tag{B3}$$

The Gibbs free energy of mixing $\overline{G}_{\mathrm{m}}^{\mathrm{mix}}(x)$ is the energy added to the mechanical mixture of the pure end-members:

$$\overline{G}_{\mathrm{m}}^{\mathrm{mix}}(x) = \mathrm{R}T(1-x)\log(1-x) + \mathrm{R}Tx\log(x) + \overline{G}_{\mathrm{m}}^{\mathrm{xs}}(x) \tag{B4}$$

Expressed with the ASF formalism, $\overline{G}_{\mathrm{m}}^{\mathrm{xs}}(x)$ reduces to:

$$\overline{G}_{\mathrm{m}}^{\mathrm{xs}}(x) = \frac{2\alpha_i\alpha_j W_{ij}(1-x)x}{(\alpha_i+\alpha_j)(\alpha_i(1-x)+\alpha_j x)} \tag{B5}$$

Note that in an ideal mixing scheme, $\overline{G}_{\mathrm{m}}^{\mathrm{xs}}(x) = 0$ and $\overline{G}_{\mathrm{m}}^{\mathrm{mix}}(x)$ is negative with a temperature-dependent minimum value at $x = 0.5$ reflecting the entropy of mixing.

781 Equilibrium implies that the chemical potential of each end-member must be
782 the same in each phase:

$$\mu_i(x)_{x=x_1} = \mu_i(x)_{x=x_2} \tag{B6}$$

$$\mu_j(x)_{x=x_1} = \mu_j(x)_{x=x_2} \tag{B7}$$

783 Using equation B1 and equation B2, we obtain the two conditions B8 and B9:

$$\frac{\delta \overline{G}_m(x_1)}{\delta x} = \frac{\delta \overline{G}_m(x_2)}{\delta x} \tag{B8}$$

784 and

$$\overline{G}_m(x_1) - \overline{G}_m(x_2) = (x_1 - x_2)\frac{\delta \overline{G}_m(x_1)}{\delta x} \tag{B9}$$

785 where

$$\begin{aligned}\frac{\delta \overline{G}_m(x)}{\delta x} = \mu_j^0 - \mu_i^0 + \mathrm{R}T\log(\frac{x}{1-x}) \\ + \frac{2\alpha_i\alpha_j W_{ij}(\alpha_i(x-1)^2 - \alpha_j x^2)}{(\alpha_i+\alpha_j)(\alpha_i(x-1)-\alpha_j x)^2}\end{aligned} \tag{B10}$$

786 In the special case of a symmetric solvus, the gradient of Gibbs energy with com-
787 position $\frac{\delta \overline{G}_m(x)}{\delta x} = 0$ at binodal compositions.

788 Combining equations B8 and B9 with equation B5 gives

$$W_{ij} = \mathrm{R}T((1-x_2)\log(\frac{1-x_2}{1-x_1}) + x_2\log(\frac{x_2}{x_1})) * D \tag{B11}$$

789 where D is given by:

$$D = -\frac{(\alpha_i+\alpha_j)(\alpha_i(x_1-1)-\alpha_j x_1)^2(\alpha_i(x_2-1)-\alpha_j x_2)}{2\alpha_i^2\alpha_j^2(x_1-x_2)^2} \tag{B12}$$

790 and

$$\alpha_j = \frac{\alpha_i(2(x_1-1)(x_2-1)\log(\frac{x_1-1}{x_2-1}) + (x_1+x_2-2x_1x_2)\log(\frac{x_1}{x_2}))}{(-x_2+x_1(2x_2-1))\log(\frac{x_1-1}{x_2-1}) - 2x_1x_2\log(\frac{x_1}{x_2})} \tag{B13}$$

Defining $\alpha_i = 1$, only one of α_i and α_j varies independently and D can be expressed as $D = E/F$, where E and F depend only on x_1 and x_2:

$$\begin{aligned} E = 2((x_1(2x_2-1)-x_2)\log(\frac{x_1-1}{x_2-1}) \\ -2x_1x_2\log(\frac{x_1}{x_2}))^2(2(x_1-1)(x_2-1)\log(\frac{x_1-1}{x_2-1}) \\ +(-2x_2x_1+x_1+x_2)\log(\frac{x_1}{x_2}))^2 \end{aligned} \tag{B14}$$

$$\begin{aligned} F = (x_2-x_1)((x_1-1)\log(\frac{x_1-1}{x_2-1}) - x_1\log(\frac{x_1}{x_2}))^2 \\ ((x_2-1)\log(\frac{x_1-1}{x_2-1}) - x_2\log(\frac{x_1}{x_2})) \\ ((-3x_2+x_1(4x_2-3)+2)\log(\frac{x_1-1}{x_2-1}) + (-4x_2x_1+x_1+x_2)\log(\frac{x_1}{x_2})) \end{aligned} \tag{B15}$$

The conditions of critical mixing (consolute point along isotherms or isobars on phase diagrams such as presented in figure 3) are reached when:

$$\frac{\delta^2\overline{G}_m(x_c)}{\delta x^2} = \frac{\mathrm{R}T_\mathrm{C}}{x_\mathrm{C}-x_\mathrm{C}^2} - \frac{4\alpha_i^2\alpha_j^2W_{ij}}{(\alpha_i+\alpha_j)(\alpha_i+x_\mathrm{C}(\alpha_j-\alpha_i))^3} = 0 \tag{B16}$$

and

$$\begin{aligned} \frac{\delta^3\overline{G}_m(x_c)}{\delta x^3} = \mathrm{R}T_\mathrm{C}(\frac{1}{(x_\mathrm{C}-1)^2} - \frac{1}{x_\mathrm{C}^2}) \\ +\frac{12\alpha_i^2\alpha_j^2W_{ij}(\alpha_j-\alpha_i)}{(\alpha_i+\alpha_j)(\alpha_i+x_\mathrm{C}(\alpha_j-\alpha_i))^4} = 0 \end{aligned} \tag{B17}$$

where T_C is the critical temperature. This defines W_{ij} as:

$$W_{ij} = \mathrm{R}T_\mathrm{C}\frac{(\alpha_i+\alpha_j)(\alpha_i(x_\mathrm{C}-1)-\alpha_jx_\mathrm{C})^3}{4\alpha_i^2\alpha_j^2(x_\mathrm{C}^2-x_\mathrm{C})} \tag{B18}$$

and α_j as

$$\alpha_j = \frac{\alpha_i(x_\mathrm{C}^2-1)}{x_\mathrm{C}(x_\mathrm{C}-2)} \tag{B19}$$

The two coexisting compositions can be calculated by minimizing the Gibbs free energy of the system (see Connolly, 2009; De Capitani and Petrakakis, 2010) or by solving equations B8 and B9 for x_1 and x_2. Equation B8 gives:

$$\frac{2\alpha_i^2\alpha_j^2 W_{ij}(x_1 - x_2)(\alpha_i(x_1 + x_2 - 2) - \alpha_j(x_1 + x_2))}{(\alpha_i + \alpha_j)(\alpha_i(x_1 - 1) + \alpha_j x_1)^2(\alpha_i(x_2 - 1) - \alpha_j x^2)} + \mathrm{R}T(\log(\frac{1 - x_2}{1 - x_1}) + \log(\frac{x_1}{x_2})) = 0 \quad \text{(B20)}$$

Equation B9 gives:

$$\frac{-2\alpha_i^2\alpha_j^2 W_{ij}(x_1 - x_2)^2}{(\alpha_i + \alpha_j)(\alpha_i(x_1 - 1) + \alpha_j x_1)^2(\alpha_i(x_2 - 1) - \alpha_j x^2)} + \mathrm{R}T((x_2 - 1)\log(\frac{1 - x_2}{1 - x_1}) + x_2\log(\frac{x_1}{x_2})) = 0 \quad \text{(B21)}$$

APPENDIX C

Measurements of the conductance of NaCl solutions are used to estimate the degree of dissociation of $NaCl^0$ into Na^+ and Cl^- (eq. 11) via:

$$x_{\mathrm{NaCl}\pm} = \Lambda\epsilon/\Lambda e \tag{C1}$$

where $x_{\mathrm{NaCl}\pm}$ is the fraction of NaCl dissolved as NaCl$\pm$, $\Lambda\epsilon$ is the experimentally determined equivalent conductance and Λe is the equivalent conductance of a hypothetical completely dissociated NaCl solution of the same effective ionic strength (Oelkers and Helgeson, 1988). Λe is calculated from the limiting equivalent conductance of the electrolyte (Λe^0). Λe for NaCl solutions has been obtained with the equation of Monica et al. (1984), which is valid up to at least 6 molal:

$$\Lambda e.\eta/\eta_0 = (\Lambda e^0 - \frac{B_2\sqrt{c}}{1 + B\mathring{a}\sqrt{c}})(1 - \frac{B_1\sqrt{c}}{1 + B\mathring{a}\sqrt{c}}\frac{e^{0.2929\kappa\alpha} - 1}{0.2929\kappa\alpha}) \tag{C2}$$

where η is the viscosity of the solution, η_0 the viscosity of the pure solvent, c the concentration of NaCl and $\mathring{a}$ the ion size parameter taken from Helgeson et al. (1981). B_1 and B_2 are coefficients originating from the formula of Onsager (1927) and modified by Monica et al. (1984) such as $B_1 = 8.2053 * 10^5\sqrt{\rho}/(\epsilon\mathrm{T})^{3/2}$ and $B_2 = 82.48\sqrt{\rho}/(\eta\sqrt{\epsilon\mathrm{T}})$, with ρ density of the solvent and ϵ dielectric constant of water. $\kappa\alpha$ is a dimensionless quantity from the Debye-Huckel formula and is calculated as:

$$\kappa\alpha = B\mathring{a}\sqrt{c} = 50.294\mathring{a}\sqrt{c}/\sqrt{\epsilon\mathrm{T}} \tag{C3}$$

Equation C2 is a refinement of the Wishaw and Stokes (1954) equation which allows correction of the ionic mobility for changing viscosity and is based on the original equations proposed for dilute solutions by Falkenhagen et al. (1952).

Oelkers and Helgeson (1988) have used the Shedlovsky equation (Shedlovsky, 1938) to estimate the degree of association in solutions up to 0.1 molal for various electrolytes. However, the Shedlovsky equation is not valid for the calculation of Λe for solutions containing more than about 0.1m. For some high-temperature conditions, the calculated values of Λe are less than the observed $\Lambda\epsilon$, leading to $x_{\mathrm{NaCl}\pm} > 1$.

Λe has been calculated for the data of Bianchi et al. (1989, 25°C, 1 bar, 0.5-3.6 molal), Chambers et al. (1956) (25°C, 1 bar, 0.1-5.35 molal) and from Quist and Marshall (1968) for solutions of 0.1molal NaCl in the range 100°C-600°C. For each experimental result, η_0 has been calculated with the IAPWS EOS of water. When not measured, η was calculated with the equation of Mao et al. (2009). The increase in viscosity for solutions of 0.1 molal NaCl or less has little impact on the calculated Λe and has been neglected for the data of Quist and Marshall (1968). The densities reported along with temperatures by Quist and Marshall (1968) were individually converted to pressures with the IAPWS EOS.

APPENDIX D

The following tables provide values and covariance matrices for coefficients used in the modeling and described in the text. The diagonal of a covariance matrix is the variance.

	Value	k1	k2	k3	k4	k5	k6	k7	k8	k9	k10	k11	k12	k13	k14	k15	k16	k17	k18	k19	k20	k21
k1	-	-	-	-	-	-	-	-	-	-	-	-	-	-	-	-	-	-	-	-	-	-
k2	3.5237E-05	-	3.14E-11	-1.32E-13	2.09E-16	-4.74E-09	7.14E-11	-4.48E-13	4.90E-16	-	-	-4.11E-08	6.68E-10	9.48E-12	-3.84E-14	4.98E-17	-	-	-4.58E-14	6.92E-17	-4.63E-12	1.15E-17
k3	-1.3772E-07	-	-1.32E-13	5.69E-16	-9.10E-19	1.78E-11	-2.67E-13	1.68E-15	-1.76E-18	-	-	1.64E-10	-2.91E-12	-3.93E-14	1.62E-16	-2.14E-19	-	-	1.77E-16	-2.57E-19	1.93E-14	-4.54E-20
k4	2.2366E-10	-	2.09E-16	-9.10E-19	1.48E-21	-2.79E-14	4.19E-16	-2.63E-18	2.73E-21	-	-	-2.51E-13	4.58E-15	6.22E-17	-2.57E-19	3.47E-22	-	-	-2.78E-19	4.01E-22	-3.03E-17	6.90E-23
k5	-2.7484E-02	-	-4.74E-09	1.78E-11	-2.79E-14	1.13E-06	-1.68E-08	1.04E-10	-1.31E-13	-	-	9.14E-06	-6.92E-08	-1.48E-09	5.65E-12	-7.04E-15	-	-	9.59E-12	-1.66E-14	6.64E-10	-2.01E-15
k6	2.8638E-04	-	7.14E-11	-2.67E-13	4.19E-16	-1.68E-08	2.58E-10	-1.61E-12	2.01E-15	-	-	-1.16E-07	1.16E-09	2.23E-11	-8.49E-14	1.05E-16	-	-	-1.48E-13	2.56E-16	-1.05E-11	3.19E-17
k7	-1.3932E-06	-	-4.48E-13	1.68E-15	-2.63E-18	1.04E-10	-1.61E-12	1.00E-14	-1.25E-17	-	-	7.08E-10	-7.37E-12	-1.40E-13	5.32E-16	-6.57E-19	-	-	9.29E-16	-1.60E-18	6.62E-14	-2.00E-19
k8	1.7538E-09	-	4.90E-16	-1.76E-18	2.73E-21	-1.31E-13	2.01E-15	-1.25E-17	1.61E-20	-	-	-9.04E-13	6.79E-15	1.54E-16	-5.74E-19	6.96E-22	-	-	-1.13E-18	2.01E-21	-7.05E-17	2.31E-22
k9	-	-	-	-	-	-	-	-	-	-	-	-	-	-	-	-	-	-	-	-	-	-
k10	-	-	-	-	-	-	-	-	-	-	-	-	-	-	-	-	-	-	-	-	-	-
k11	2.5909E-02	-	-4.11E-08	1.64E-10	-2.51E-13	9.14E-06	-1.16E-07	7.08E-10	-9.04E-13	-	-	1.40E-04	-3.74E-07	-1.24E-08	4.89E-11	-6.33E-14	-	-	6.34E-11	-1.12E-13	4.30E-09	-1.23E-14
k12	7.8597E-04	-	6.68E-10	-2.91E-12	4.58E-15	-6.92E-08	1.16E-09	-7.37E-12	6.79E-15	-	-	-3.74E-07	1.99E-08	1.90E-10	-7.99E-13	1.03E-15	-	-	-8.33E-13	1.10E-15	-1.12E-10	2.66E-16
k13	9.7084E-06	-	9.48E-12	-3.93E-14	6.22E-17	-1.48E-09	2.23E-11	-1.40E-13	1.54E-16	-	-	-1.24E-08	1.90E-10	2.95E-12	-1.18E-14	1.52E-17	-	-	-1.42E-14	2.16E-17	-1.40E-12	3.49E-18
k14	-4.1348E-08	-	-3.84E-14	1.62E-16	-2.57E-19	5.65E-12	-8.49E-14	5.32E-16	-5.74E-19	-	-	4.89E-11	-7.99E-13	-1.18E-14	4.78E-17	-6.22E-20	-	-	5.49E-17	-8.19E-20	5.65E-15	-1.38E-20
k15	5.2823E-11	-	4.98E-17	-2.14E-19	3.47E-22	-7.04E-15	1.05E-16	-6.57E-19	6.96E-22	-	-	-6.33E-14	1.03E-15	1.52E-17	-6.22E-20	8.31E-23	-	-	-6.85E-20	1.01E-22	-7.18E-18	1.67E-23
k16	-	-	-	-	-	-	-	-	-	-	-	-	-	-	-	-	-	-	-	-	-	-
k17	-	-	-	-	-	-	-	-	-	-	-	-	-	-	-	-	-	-	-	-	-	-
k18	-9.7539E-08	-	-4.58E-14	1.77E-16	-2.78E-19	9.59E-12	-1.48E-13	9.29E-16	-1.13E-18	-	-	6.34E-11	-8.33E-13	-1.42E-14	5.49E-17	-6.85E-20	-	-	8.83E-17	-1.47E-19	6.89E-15	-1.98E-20
k19	1.8277E-10	-	6.92E-17	-2.57E-19	4.01E-22	-1.66E-14	2.56E-16	-1.60E-18	2.01E-21	-	-	-1.12E-13	1.10E-15	2.16E-17	-8.19E-20	1.01E-22	-	-	-1.47E-19	2.55E-22	-1.02E-17	3.13E-23
k20	-5.7627E-06	-	-4.63E-12	1.93E-14	-3.03E-17	6.64E-10	-1.05E-11	6.62E-14	-7.05E-17	-	-	4.30E-09	-1.12E-10	-1.40E-12	5.65E-15	-7.18E-18	-	-	6.89E-15	-1.02E-17	7.39E-13	-1.86E-18
k21	2.2035E-11	-	1.15E-17	-4.54E-20	6.90E-23	-2.01E-15	3.19E-17	-2.00E-19	2.31E-22	-	-	-1.23E-14	2.66E-16	3.49E-18	-1.38E-20	1.67E-23	-	-	-1.98E-20	3.13E-23	-1.86E-18	5.32E-24

Table D1: Values of parameters and associated covariance matrix for equations 8 and 9 for $W_{\mathrm{H_2O\text{-}CO_2}}/\mathrm{R}T$.

	Value	j1	j2	j3	j4	j5	j6	j7	j8	j9	j10	j11	j12	j13	j14	j15	j16	j17	j18	j19	j20	j21
j1	-4.5946E-02	8.70E-05	1.19E-06	9.89E-10	-9.97E-13	-	1.82E-08	-6.80E-11	6.69E-14	-9.86E-08	-4.14E-12	5.24E-04	-8.27E-05	1.08E-06	-	-	-2.75E-06	3.08E-09	-	6.68E-15	4.02E-07	-
j2	-7.6283E-04	1.19E-06	2.54E-08	1.90E-11	-1.79E-14	-	1.35E-10	-3.18E-13	1.31E-16	-9.90E-10	-9.06E-14	2.42E-05	-1.78E-06	2.23E-08	-	-	-1.62E-07	2.92E-10	-	-1.92E-16	7.61E-09	-
j3	-6.2299E-07	9.89E-10	1.90E-11	1.54E-14	-1.54E-17	-	1.11E-13	-2.68E-16	1.17E-19	-8.98E-13	-6.78E-17	1.76E-08	-1.34E-09	1.69E-11	-	-	-1.19E-10	2.19E-13	-	-1.51E-19	5.87E-12	-
j4	6.1752E-10	-9.97E-13	-1.79E-14	-1.54E-17	1.59E-20	-	-1.17E-16	3.01E-19	-1.59E-22	9.45E-16	6.39E-20	-1.62E-11	1.28E-12	-1.61E-14	-	-	1.10E-13	-2.03E-16	-	1.37E-22	-5.67E-15	-
j5	-	-	-	-	-	-	-	-	-	-	-	-	-	-	-	-	-	-	-	-	-	-
j6	-4.5659E-05	1.82E-08	1.35E-10	1.11E-13	-1.17E-16	-	9.01E-12	-4.10E-14	4.80E-17	-2.54E-11	-4.39E-16	-2.93E-07	-7.97E-09	1.25E-10	-	-	2.82E-09	-7.17E-12	-	1.27E-17	5.50E-11	-
j7	1.4810E-07	-6.80E-11	-3.18E-13	-2.68E-16	3.01E-19	-	-4.10E-14	1.92E-16	-2.31E-19	1.04E-13	9.46E-19	1.76E-09	1.38E-11	-3.08E-13	-	-	-1.62E-11	3.98E-14	-	-6.63E-20	-1.53E-13	-
j8	-1.3101E-10	6.69E-14	1.31E-16	1.17E-19	-1.59E-22	-	4.80E-17	-2.31E-19	2.81E-22	-1.11E-16	-2.43E-22	-2.42E-12	2.31E-15	1.45E-16	-	-	2.18E-14	-5.29E-17	-	8.55E-23	9.73E-17	-
j9	4.3745E-05	-9.86E-08	-9.90E-10	-8.98E-13	9.45E-16	-	-2.54E-11	1.04E-13	-1.11E-16	1.29E-10	3.38E-15	2.51E-07	6.51E-08	-9.27E-10	-	-	-3.18E-09	9.58E-12	-	-2.33E-17	-3.58E-10	-
j10	2.7152E-09	-4.14E-12	-9.06E-14	-6.78E-17	6.39E-20	-	-4.39E-16	9.46E-19	-2.43E-22	3.38E-15	3.24E-19	-8.68E-11	6.31E-12	-7.93E-14	-	-	5.84E-13	-1.06E-15	-	7.35E-22	-2.69E-14	-
j11	-6.3984E-01	5.24E-04	2.42E-05	1.76E-08	-1.62E-11	-	-2.93E-07	1.76E-09	-2.42E-12	2.51E-07	-8.68E-11	5.95E-02	-2.03E-03	2.11E-05	-	-	-4.51E-04	9.48E-07	-	-1.15E-12	7.51E-06	-
j12	5.5016E-02	-8.27E-05	-1.78E-06	-1.34E-09	1.28E-12	-	-7.97E-09	1.38E-11	2.31E-15	6.51E-08	6.31E-12	-2.03E-03	1.30E-04	-1.57E-06	-	-	1.39E-05	-2.59E-08	-	2.03E-14	-5.53E-07	-
j13	-6.7895E-04	1.08E-06	2.23E-08	1.69E-11	-1.61E-14	-	1.25E-10	-3.08E-13	1.45E-16	-9.27E-10	-7.93E-14	2.11E-05	-1.57E-06	1.96E-08	-	-	-1.41E-07	2.54E-10	-	-1.64E-16	6.75E-09	-
j14	-	-	-	-	-	-	-	-	-	-	-	-	-	-	-	-	-	-	-	-	-	-
j15	-	-	-	-	-	-	-	-	-	-	-	-	-	-	-	-	-	-	-	-	-	-
j16	5.2944E-03	-2.75E-06	-1.62E-07	-1.19E-10	1.10E-13	-	2.82E-09	-1.62E-11	2.18E-14	-3.18E-09	5.84E-13	-4.51E-04	1.39E-05	-1.41E-07	-	-	3.51E-06	-7.58E-09	-	9.71E-15	-5.02E-08	-
j17	-1.1929E-05	3.08E-09	2.92E-10	2.19E-13	-2.03E-16	-	-7.17E-12	3.98E-14	-5.29E-17	9.58E-12	-1.06E-15	9.48E-07	-2.59E-08	2.54E-10	-	-	-7.58E-09	1.68E-11	-	-2.26E-17	9.09E-11	-
j18	-	-	-	-	-	-	-	-	-	-	-	-	-	-	-	-	-	-	-	-	-	-
j19	1.4402E-11	6.68E-15	-1.92E-16	-1.51E-19	1.37E-22	-	1.27E-17	-6.63E-20	8.55E-23	-2.33E-17	7.35E-22	-1.15E-12	2.03E-14	-1.64E-16	-	-	9.71E-15	-2.26E-17	-	3.34E-23	-5.86E-17	-
j20	-2.5360E-04	4.02E-07	7.61E-09	5.87E-12	-5.67E-15	-	5.50E-11	-1.53E-13	9.73E-17	-3.58E-10	-2.69E-14	7.51E-06	-5.53E-07	6.75E-09	-	-	-5.02E-08	9.09E-11	-	-5.86E-17	2.43E-09	-
j21	-	-	-	-	-	-	-	-	-	-	-	-	-	-	-	-	-	-	-	-	-	-

Table D2: Values of parameters and associated covariance matrix for equations 8 and 9 for α_{CO_2}.

	Value	C1	C2	C3	C4	C5	C6	C7	C8	C9	C10	C11	C12
C1	-3.95E00	1.05E00	-1.21E-01	2.89E-04	-3.66E-07	-	-3.79E-03	3.23E-01	1.70E-02	-8.69E-03	3.20E-04	-2.30E-04	3.04E-07
C2	-1.06E00	-1.21E-01	1.39E-02	-3.29E-05	4.15E-08	-	4.35E-04	-3.66E-02	-1.93E-03	9.86E-04	-3.62E-05	2.62E-05	-3.45E-08
C3	-6.20E-03	2.89E-04	-3.29E-05	8.08E-08	-1.03E-10	-	-1.04E-06	9.10E-05	4.77E-06	-2.45E-06	9.06E-08	-6.42E-08	8.51E-11
C4	3.77E-05	-3.66E-07	4.15E-08	-1.03E-10	1.33E-13	-	1.31E-09	-1.17E-07	-6.12E-09	3.15E-09	-1.17E-10	8.20E-11	-1.09E-13
C5	1.64E00	-	-	-	-	-	-	-	-	-	-	-	-
C6	-1.02E-01	-3.79E-03	4.35E-04	-1.04E-06	1.31E-09	-	1.38E-05	-1.15E-03	-6.07E-05	3.11E-05	-1.14E-06	8.26E-07	-1.09E-09
C7	-1.03E01	3.23E-01	-3.66E-02	9.10E-05	-1.17E-07	-	-1.15E-03	1.03E-01	5.39E-03	-2.77E-03	1.03E-04	-7.22E-05	9.61E-08
C8	-7.55E-01	1.70E-02	-1.93E-03	4.77E-06	-6.12E-09	-	-6.07E-05	5.39E-03	2.83E-04	-1.45E-04	5.37E-06	-3.78E-06	5.02E-09
C9	8.97E-01	-8.69E-03	9.86E-04	-2.45E-06	3.15E-09	-	3.11E-05	-2.77E-03	-1.45E-04	7.47E-05	-2.77E-06	1.95E-06	-2.59E-09
C10	1.11E-03	3.20E-04	-3.62E-05	9.06E-08	-1.17E-10	-	-1.14E-06	1.03E-04	5.37E-06	-2.77E-06	1.03E-07	-7.22E-08	9.64E-11
C11	-1.67E-03	-2.30E-04	2.62E-05	-6.42E-08	8.20E-11	-	8.26E-07	-7.22E-05	-3.78E-06	1.95E-06	-7.22E-08	5.15E-08	-6.87E-11
C12	1.71E00	3.04E-07	-3.45E-08	8.51E-11	-1.09E-13	-	-1.09E-09	9.61E-08	5.02E-09	-2.59E-09	9.64E-11	-6.87E-11	9.24E-14

Table D3: Values and covariance matrices for C_1 to C_{12} (equations 13 to 16).

	Value	D1	D2	D3	D4	D5
D1	3.92E01	1.50E00	-2.15E-01	-4.56E-03	8.92E-04	-1.61E-02
D2	-1.04E00	-2.15E-01	5.29E-02	4.85E-04	-1.06E-04	-8.00E-04
D3	-1.29E-01	-4.56E-03	4.85E-04	1.56E-05	-3.07E-06	8.16E-05
D4	2.03E-02	8.92E-04	-1.06E-04	-3.07E-06	6.51E-07	-1.77E-05
D5	-6.41E-01	-1.61E-02	-8.00E-04	8.16E-05	-1.77E-05	8.82E-04

Table D4: Values and covariance matrices for D_1 to D_5 (equation 17).

841 Adams L.H. (1931) Equilibrium in Binary Systems Under Pressure. I. An Ex-
842 perimental and Thermodynamic Investigation of the System NaCl-H_2O, at 25
843 degres. *Journal of American Chemical Society* **53**, 3769–3813.

844 Akinfiev N.N. and Diamond L.W. (2010) Thermodynamic model of aqueous CO_2-
845 H_2O-NaCl solutions from -22 to 100 °C and from 0.1 to 100 MPa. *Fluid Phase*
846 *Equilibria* **295**, 104 – 124. doi:10.1016/j.fluid.2010.04.007.

847 Anderson G. and Crerar D. (1993) Thermodynamics in geochemistry: The equi-
848 librium model p. 588.

849 Anderson G., Castet S., Schott J. and Mesmer R. (1991) The density model
850 for estimation of thermodynamic parameters of reactions at high temperatures
851 and pressures. *Geochimica et Cosmochimica Acta* **55**, 1769 – 1779. doi:
852 10.1016/0016-7037(91)90022-W.

853 Anderson G.K. (2002) Solubility of carbon dioxide in water under incipient
854 clathrate formation conditions. *Journal of Chemical and Engineering Data*
855 **47**, 219–222. doi:10.1021/je015518c.

856 Angiboust S., Wolf S., Burov E., Agard P. and Yamato P. (2012) Effect of fluid
857 circulation on subduction interface tectonic processes: Insights from thermo-
858 mechanical numerical modelling. *Earth and Planetary Science Letters* **357-**
859 **358**, 238 – 248. doi:10.1016/j.epsl.2012.09.012.

860 Aranovich L. and Newton R. (1996) H_2O activity in concentrated NaCl solutions
861 at high pressures and temperatures measured by the brucite-periclase equilib-
862 rium. *Contributions to Mineralogy and Petrology* **125**, 200–212.

Aranovich L.Y. and Berman R.G. (1996) Optimized standard state and solution properties of minerals. *Contributions to Mineralogy and Petrology* **126**, 25–37. 10.1007/s004100050233.

Aranovich L.Y. and Newton R.C. (1999) Experimental determination of CO_2-H_2O activity-composition relations at 600-1000 degrees C and 6-14 kbar by reversed decarbonation and dehydration reactions. *American Mineralogist* **84**, 1319–1332.

Bamberger A., Sieder G. and Maurer G. (2000) High-pressure (vapor+liquid) equilibrium in binary mixtures of (carbon dioxide+water or acetic acid) at temperatures from 313 to 353 K. *The Journal of Supercritical Fluids* **17**, 97 – 110. doi:10.1016/S0896-8446(99)00054-6.

Bartholomé E. and Friz H. (1956) Solubility of CO_2 in water. *Chem. Ing. Tech* . **28**, 706–708.

Becker J.A., Bickle M.J., Galy A. and Holland T.J. (2008) Himalayan metamorphic CO_2 fluxes: Quantitative constraints from hydrothermal springs. *Earth and Planetary Science Letters* **265**, 616 – 629. doi:10.1016/j.epsl.2007.10.046.

Berman R. (1988) Internally-consistent thermodynamic data for minerals in the system Na_2O-K_2O-CaO-MgO-FeO-Fe_2O_3-Al_2O_3-SiO_2-TiO_2-H_2O-CO_2. *Journal of Petrology* **29**, 445–522.

Berman R.G. and Aranovich L.Y. (1996) Optimized standard state and solution properties of minerals. *Contributions to Mineralogy and Petrology* **126**, 1–24. 10.1007/s004100050232.

885 Bevington P. and Robinson D. (2002) *Data Reduction and Error Analysis for The*
886 *Physical Sciences*. McGraw-Hill Higher Education, 3 edn.

887 Bianchi H., Corti H.R. and Fernndez-Prini R. (1989) The conductivity of con-
888 centrated aqueous mixtures of NaCl and $MgCl_2$ at 25°C˙ *Journal of Solution*
889 *Chemistry* **18**, 485–491. doi:10.1007/BF00657336.

890 Bickle M.J. (2009) Geological carbon storage. *Nature Geoscience* **2**, 815–818.
891 doi:10.1038/ngeo687.

892 Bodnar R. (1994) Synthetic fluid inclusions: XII. The system H2ONaCl. Experi-
893 mental determination of the halite liquidus and isochores for a 40 wt% NaCl so-
894 lution. *Geochimica et Cosmochimica Acta* **58**, 1053 – 1063. doi:10.1016/0016-
895 7037(94)90571-1.

896 Chambers J.F., Stokes J.M. and Stokes R.H. (1956) Conductances of Concentrated
897 Aqueous Sodium and Potassium Chloride Solutions at 25°C˙ *The Journal of*
898 *Physical Chemistry* **60**, 985–986. doi:10.1021/j150541a040.

899 Chapman W., Gubbins K., Jackson G. and Radosz M. (1989) SAFT: Equation-of-
900 state solution model for associating fluids. *Fluid Phase Equilibria* **52**, 31 – 38.
901 doi:10.1016/0378-3812(89)80308-5.

902 Chester F., Evans J. and Biegel R. (1993) Internal Structure and Weakening Mech-
903 anisms Of The San-Andreas Fault. *Journal of Geophysical Research-Solid*
904 *Earth* **98**, 771–786.

905 Clegg S.L. and Pitzer K.S. (1992) Thermodynamics of multicomponent, misci-
906 ble, ionic solutions: generalized equations for symmetrical electrolytes. *The*
907 *Journal of Physical Chemistry* **96**, 3513–3520. doi:10.1021/j100187a061.

Clegg S.L., Pitzer K.S. and Brimblecombe P. (1992) Thermodynamics of multicomponent, miscible, ionic solutions. Mixtures including unsymmetrical electrolytes. *The Journal of Physical Chemistry* **96**, 9470–9479. doi: 10.1021/j100202a074.

Clynne M.A., Potter R.W. and Haas J.L. (1981) Solubility of sodium chloride in aqueous electrolyte solutions from 10 to 100 degrees C. *Journal of Chemical & Engineering Data* **26**, 396–398. doi:10.1021/je00026a014.

Connolly J.A.D. (2009) The geodynamic equation of state: What and how. *Geochemistry Geophysics Geosystems* **10**. doi:10.1029/2009GC002540.

Cotterman R.L. and Prausnitz J.M. (1986) Molecular thermodynamics for fluids at low and high densities. Part II: Phase equilibria for mixtures containing components with large differences in molecular size or potential energy. *AIChE Journal* **32**, 1799–1812. doi:10.1002/aic.690321105.

De Capitani C. and Peters T. (1982) Corresponding states in binary solutions and graphical determination of Margules parameters. *Contributions to Mineralogy and Petrology* **81**, 48–58.

De Capitani C. and Petrakakis K. (2010) The computation of equilibrium assemblage diagrams with Theriak/Domino software. *American Mineralogist* **95**, 1006–1016. doi:10.2138/am.2010.3354.

Debye P. and Hückel E. (1923a) The theory of electrolytes I. The lowering of the freezing point and related occurrences. *Physikalische Zeitschrift* **24**, 185–206.

Debye P. and Hückel E. (1923b) The theory of the electrolyte II - The border law for electrical conductivity. *Physikalische Zeitschrift* **24**, 305–325.

931 Diamond L.W. and Akinfiev N.N. (2003) Solubility of CO_2 in water from -1.5 to
932 100 °C and from 0.1 to 100 MPa: evaluation of literature data and thermody-
933 namic modelling. *Fluid Phase Equilibria* **208**, 265 – 290. doi:10.1016/S0378-
934 3812(03)00041-4.

935 Driesner T. (2007) The system H2O-NaCl. Part II: Correlations for molar vol-
936 ume, enthalpy, and isobaric heat capacity from 0 to 1000°C, 1 to 5000 bar,
937 and 0 to 1 XNaCl. *Geochimica et Cosmochimica Acta* **71**, 4902 – 4919. doi:
938 10.1016/j.gca.2007.05.026.

939 Driesner T. and Heinrich C.A. (2007) The system H_2O-NaCl. Part I: Correlation
940 formulae for phase relations in temperature-pressure-composition space from
941 0 to 1000°C, 0 to 5000 bar, and 0 to 1 XNaCl. *Geochimica et Cosmochimica*
942 *Acta* **71**, 4880 – 4901. doi:10.1016/j.gca.2006.01.033.

943 Drummond S. (1981) *Boiling and mixing of hydrothermal fluids : chemical effects*
944 *on mineral precipitation*. Ph.D. thesis, Pennsylvannia States University.

945 Duan Z. and Li D. (2008) Coupled phase and aqueous species equilibrium of the
946 H_2O-CO_2-NaCl-$CaCO_3$ system from 0 to 250 °C, 1 to 1000 bar with NaCl
947 concentrations up to saturation of halite. *Geochimica et Cosmochimica Acta*
948 **72**, 5128 – 5145. doi:10.1016/j.gca.2008.07.025.

949 Duan Z. and Sun R. (2003) An improved model calculating CO_2 solubility in pure
950 water and aqueous NaCl solutions from 273 to 533 K and from 0 to 2000 bar.
951 *Chemical Geology* **193**, 257 – 271. doi:10.1016/S0009-2541(02)00263-2.

952 Duan Z. and Zhang Z. (2006) Equation of state of the H_2O-CO_2 system up to

953 10 GPa and 2573K: Molecular dynamics simulations with ab initio potential
954 surface. *Geochimica et Cosmochimica Acta* **70**, 2311–2324.

955 Duan Z., Møller N. and Weare J.H. (1992) An equation of state for the CH_4-CO_2-
956 H_2O system: II. Mixtures from 50 to 1000°C and 0 to 1000 bar. *Geochimica et*
957 *Cosmochimica Acta* **56**, 2619 – 2631. doi:10.1016/0016-7037(92)90348-M.

958 Duan Z., Møller N. and Weare J.H. (1995) Equation of state for the NaCl-
959 H_2O-CO_2 system: prediction of phase equilibria and volumetric properties.
960 *Geochimica et Cosmochimica Acta* **59**, 2869 – 2882. doi:10.1016/0016-
961 7037(95)00182-4.

962 Duan Z., Møller N. and Weare J. (1996) A general equation of state for super-
963 critical fluids and molecular dynamics simulation of mixture PVTX properties.
964 *Geochimica et Cosmochimica Acta* **60**, 1209–1216.

965 Duan Z., Møller N. and Weare J. (2000) Accurate prediction of thermodynamic
966 properties of fluids in the system H_2O-CO_2-CH_4-N2. *Geochimica et Cos-*
967 *mochimica Acta* **64**, 1069–1075. doi:10.1016/S0016-7037(99)00368-3.

968 Duan Z., Møller N. and Weare J. (2003) Equations of State for the NaCl-H_2O-CH_4
969 System and the NaCl-H_2O-CO_2-CH_4 System: Phase Equilibria and Volumetric
970 Properties above 573 K. *Geochimica et Cosmochimica Acta* **67**, 671–680. doi:
971 10.1016/S0016-7037(02)01226-7.

972 Duan Z., Sun R. and Zhu C. (2006) An improved model for the calculation of
973 CO_2 solubility in aqueous solutions containing Na^+, K^+, Ca^{2+}, Mg^{2+}, Cl^-, and
974 SO_4^{2-}. *Marine Chemistry* **98**, 131–139. doi:10.1016/j.marchem.2005.09.001.

975 Duan Z., Hu J., Li D. and Mao S. (2008) Densities of the CO_2-H_2O and CO_2-H_2O-
976 NaCl Systems Up to 647 K and 100 MPa. *Energy & Fuels* **22**, 1666–1674.

977 Edmond J., Measures C., McDuff R., Chan L., Collier R., Grant B., Gordon L.
978 and Corliss J. (1979) Ridge crest hydrothermal activity and the balances of
979 the major and minor elements in the ocean: The Galapagos data. *Earth and*
980 *Planetary Science Letters* **46**, 1 – 18. doi:10.1016/0012-821X(79)90061-X.

981 Ellis A. and Golding R. (1963) Solubility of carbon dioxide above 100°C in water
982 and in sodium chloride solutions. *American Journal of Science* **261**, 47–60.

983 Evans K. and Powell R. (2006) A method for activity calculations in saline and
984 mixed solvent solutions at elevated temperature and pressure: A framework for
985 geological phase equilibria calculations. *Geochimica et cosmochimica acta* **70,**
986 **22**, pp. 5488–5506. doi:10.1016/j.gca.2006.08.032.

987 Evans K. and Powell R. (2007) DES-code: A metacode to aid calculation of the
988 chemical potential of aqueous solutions at elevated temperatures and pressures.
989 *Computers and Geosciences* **33**, 789–807. doi:10.1016/j.cageo.2006.09.010.

990 Evans K.A., Powell R. and Holland T.J.B. (2010) Internally consistent data
991 for sulphur-bearing phases and application to the construction of pseudosec-
992 tions for mafic greenschist facies rocks in Na_2O-CaO-K_2O-FeO-MgO-Al_2O_3-
993 SiO_2-CO_2-O-S-H_2O. *Journal of Metamorphic Geology* **28**, 667–687. doi:
994 10.1111/j.1525-1314.2010.00890.x.

995 Falkenhagen H., Leist M. and Kelbg G. (1952) Zur Theorie der Leitfhigkeit
996 starker nicht assoziierender Elektrolyte bei hheren Konzentrationen. *Annalen*
997 *der Physik* **446**, 51–59. doi:10.1002/andp.19524460110.

998 Farelo F., Vonbrachel G. and Offermann H. (1993) Solid liquid equilibria in the
999 ternary system NaCl-KCl-H_2O. *Canadian Journal of Chemical Engineering*
1000 **71**, 141–146.

1001 Ferry J.M. (1984) A Biotite Isograd in South-Central Maine, U.S.A.: Mineral
1002 Reactions, Fluid Transfer, and Heat Transfer. *Journal of Petrology* **25**, 871–
1003 893. doi:10.1093/petrology/25.4.871.

1004 Flowers G.C. (1979) Correction of Holloway's (1977) adaptation of the modified
1005 Redlich-Kwong equation of state for calculation of the fugacities of molecular
1006 species in supercritical fluids of geologic interest. *Contributions to Mineralogy*
1007 *and Petrology* **69**, 315–318. doi:10.1007/BF00372333.

1008 García A., Thomsen K. and Stenby E. (2006) Prediction of mineral scale for-
1009 mation in geothermal and oilfield operations using the Extended UNIQUAC
1010 model: Part II. Carbonate-scaling minerals. *Geothermics* **35**, 239 – 284. doi:
1011 10.1016/j.geothermics.2006.03.001.

1012 Gillespie P. and Wilson G. (1982) Vaporliquid and liquidliquid equilibria:
1013 watermethane, watercarbon dioxide, waterhydrogen sulfide, watern-pentane,
1014 watermethanen-pentane. *Gas Processors Association, Tulsa, Research Report*
1015 *RR48* .

1016 Grant-Taylor D.F. (1981) Partial molar volumes of sodium chloride solutions at
1017 200 bar, and temperatures from 175 to 350°C˙ *Journal of Solution Chemistry*
1018 **10**, 621–630. doi:10.1007/BF00650738.

1019 Greenwood H. (1967) Wollastonite: Stability in H_2O-CO_2 mixtures and oc-

curence in a contact-metamorphic aureole near Salmo, British Columbia, Canada. *American Mineralogist* **52**, 1669–1680.

Guggenheim E. (1977) *Thermodynamics*. North-Holland Publishing Company, Amsterdam.

Hacker B., Abers G. and Peacock S. (2003) Subduction factory - 1. Theoretical mineralogy, densities, seismic wave speeds, and H_2O contents. *Journal of Geophysical Research - Solid Earth* **108**. doi:10.1029/2001JB001127.

Hähnel O. (1920) Solubility of carbon dioxide in water. *Centr. Min. Geol.* **25**, 25–32.

Helgeson H.C., Kirkham D.H. and Flowers G.C. (1981) Theoretical prediction of the thermodynamic behavior of aqueous electrolytes at high pressures and temperatures: IV. Calculation of activity coefficients, osmotic coeffcients, and apparent molal and standard and relative partial molal properties to 600C and 5kb. *American Journal of Science* **281**, 1249–1516.

Hellmann R. and Tisserand D. (2006) Dissolution kinetics as a function of the Gibbs free energy of reaction: An experimental study based on albite feldspar. *Geochimica et Cosmochimica Acta* **70**, 364 – 383. doi: 10.1016/j.gca.2005.10.007.

Hnedkovský L., Wood R.H. and Majer V. (1996) Volumes of aqueous solutions of CH_4, CO_2, H_2S and NH_3 at temperatures from 298.15 K to 705 K and pressures to 35 MPa. *The Journal of Chemical Thermodynamics* **28**, 125 – 142. doi: 10.1006/jcht.1996.0011.

1042 Holland T. and Powell R. (1991) A compensated Redlich-Kwong (CORK) equa-
1043 tion for volumes and fugacities of CO_2 and H_2O in the range 1 bar to 50 kbar
1044 and 100-1600 degrees C. *Contributions to Mineralogy and Petrology* **109**, 265–
1045 273.

1046 Holland T. and Powell R. (2003) Activity-composition relations for phases in
1047 petrological calculations: an asymmetric multicomponent formulation. *Con-*
1048 *tributions to Mineralogy and Petrology* **145, 4**, 492–501. doi:10.1007/s00410-
1049 003-0464-z.

1050 Holland T.J.B. and Powell R. (1990) An enlarged and updated internally con-
1051 sistent thermodynamic dataset with uncertainties and correlations - the system
1052 K_2O-Na_2O-CaO-MgO-MnO-FeO-FE_2O_3-Al_2O_3-TiO_2-SiO_2-C-H_2-O_2. *Journal*
1053 *of Metamorphic Geology* **8**, 89–124. doi:10.1111/j.1525-1314.1990.tb00458.x.

1054 Holland T.J.B. and Powell R. (1998) An internally consistent thermodynamic data
1055 set for phases of petrological interest. *Journal of Metamorphic Geology* **16, 3**,
1056 309–343. doi:10.1111/j.1525-1314.1998.00140.x.

1057 Holland T.J.B. and Powell R. (2011) An improved and extended internally consis-
1058 tent thermodynamic dataset for phases of petrological interest, involving a new
1059 equation of state for solids. *Journal of Metamorphic Geology* **29**, 333–383.
1060 doi:10.1111/j.1525-1314.2010.00923.x.

1061 Hu J., Duan Z., Zhu C. and Chou I.M. (2007) PVTx properties of the CO_2-
1062 H_2O and CO_2-H_2O-NaCl systems below 647 K: Assessment of experimental
1063 data and thermodynamic models. *Chemical Geology* **238**, 249 – 267. doi:
1064 10.1016/j.chemgeo.2006.11.011.

Ji X. and Zhu C. (2012) A SAFT equation of state for the quaternary H_2S-CO_2-H_2O-NaCl system. *Geochimica et Cosmochimica Acta* **91**, 40 – 59. doi: 10.1016/j.gca.2012.05.023.

Ji X., Tan S.P., Adidharma H. and Radosz M. (2005) SAFT1-RPM Approximation Extended to Phase Equilibria and Densities of CO_2-H_2O and CO_2-H_2O-NaCl Systems. *Industrial & Engineering Chemistry Research* **44**, 8419–8427. doi: 10.1021/ie050725h.

Johnson E.L. (1991) Experimentally determined limits for H_2O-CO_2-NaCl immiscibility in granulites. *Geology* **19**, 925–928. doi:10.1130/0091-7613(1991)019<0925:EDLFHO>2.3.CO;2.

Joyce D.B. and Holloway J.R. (1993) An experimental determination of the thermodynamic properties of H_2O-CO_2-NaCl fluids at high pressures and temperatures. *Geochimica et Cosmochimica Acta* **57**, 733 – 746. doi:10.1016/0016-7037(93)90165-S.

Kampman N., Bickle M., Becker J., Assayag N. and Chapman H. (2009) Feldspar dissolution kinetics and Gibbs free energy dependence in a CO_2-enriched groundwater system, Green River, Utah. *Earth and Planetary Science Letters* **284**, 473 – 488. doi:10.1016/j.epsl.2009.05.013.

Keevil N.B. (1942) Vapor Pressures of Aqueous Solutions at High Temperatures. *Journal of the American Chemical Society* **64**, 841–850.

Kerrick D.M. and Caldeira K. (1998) Metamorphic CO_2 degassing from orogenic belts. *Chemical Geology* **145**, 213 – 232. doi:10.1016/S0009-2541(97)00144-7.

Kiepe J., Horstmann S., Fischer K. and Gmehling J. (2002) Experimental determination and prediction of gas solubility data for CO_2 + H_2O mixtures containing NaCl or KCl at temperatures between 313 and 393 K and pressures up to 10 MPa. *Industrial & Engineering Chemistry Research* **41**, 4393–4398. doi:10.1021/ie020154i.

King M.B., Mubarak A., Kim J.D. and Bott T.R. (1992) The mutual solubilities of water with supercritical and liquid carbon dioxides. *The Journal of Supercritical Fluids* **5**, 296 – 302. doi:10.1016/0896-8446(92)90021-B.

Kritschewsky I., Shaworonkoff N. and Aepelbaum V. (1935) Combined solubility of gases in liquids under pressure I Solubility of carbon dioxide in water from its mixtures with hydrogen of 20 and 30 degrees C and total pressure of 30 kg/cm(2). *Zeitschrift Fur Physikalische Chemie-Abteilung A-Chemische Thermodynamik Kinetik Elektrochemie Eigenschaftslehre* **175**, 232–238.

Le Bayon R., de Capitani C. and Frey M. (2006) Modelling phase-assemblage diagrams for magnesian metapelites in the system K_2O-FeO-MgO-Al_2O_3-SiO_2-H_2O: geodynamic consequences for the Monte Rosa nappe, Western Alps. *Contributions to Mineralogy and Petrology* **151**, 395–412. doi:10.1007/s00410-006-0067-6.

Levenberg K. (1944) A Method for the Solution of Certain Non-Linear Problems in Least Squares. *The Quarterly of Applied Mathematics* **2**, 164168.

Li D. and Duan Z. (2007) The speciation equilibrium coupling with phase equilibrium in the H_2O-CO_2-NaCl system from 0 to 250 °C, from 0 to 1000 bar,

and from 0 to 5 molality of NaCl. *Chemical Geology* **244**, 730 – 751. doi: 10.1016/j.chemgeo.2007.07.023.

Li Z., Dong M., Li S. and Dai L. (2004) Densities and Solubilities for Binary Systems of Carbon Dioxide + Water and Carbon Dioxide + Brine at 59°Cand Pressures to 29 MPa. *Journal of Chemical & Engineering Data* **49**, 1026–1031. doi:10.1021/je049945c.

L'Vov S., Zarembo V. and Gilyarov V. (1981) High-precision study of volume properties of water solutions of sodium-chloride under high parameters. *Geokhimiya* pp. 505–516.

Malinin S. and Kurovskaya N. (1975) Investigation of CO_2 solubility in solutions of chlorides at elevated-temperatures and pressures of CO_2. *Geokhimiya* pp. 547–550.

Malinin S. and Saveleva N. (1972) Experimental investigations of CO_2 solubility in NaCl and $CaCl_2$ solutions at temperatures of 25, 50 and 75 degrees and elevated CO_2 pressure. *Geokhimiya* pp. 643–&.

Mao S. and Duan Z. (2008) The P, V, T,x properties of binary aqueous chloride solutions up to T = 573 K and 100 MPa. *The Journal of Chemical Thermodynamics* **40**, 1046 – 1063. doi:10.1016/j.jct.2008.03.005.

Mao S. and Duan Z. (2009) The Viscosity of Aqueous Alkali-Chloride Solutions up to 623 K, 1,000 bar, and High Ionic Strength. *International Journal of Thermophysics* **30**, 1510–1523. doi:10.1007/s10765-009-0646-7.

Mao S., Duan Z. and Hu W. (2009) A vapor - liquid phase equilibrium model for binary CO_2 - H_2O and CH_4-H_2O systems above 523K for application

to fluid inclusions. *The Journal of Supercritical Fluids* **50**, 13 – 21. doi: 10.1016/j.supflu.2009.02.007.

Markham A.E. and Kobe K.A. (1941) The Solubility of Carbon Dioxide and Nitrous Oxide in Aqueous Salt Solutions. *Journal of American Chemical Society* **63**, 449–454.

Marquardt D.W. (1963) An Algorithm for Least-Squares Estimation of Nonlinear Parameters. *Journal of the Society for Industrial and Applied Mathematics* **11**, pp. 431–441.

Mather A. and Franck E. (1992) Phase-equilibria in the system carbon dioxide - water at elevated pressures. *Journal of Physical Chemistry* **96**, 6–8.

Matous J., Sobr J., Novak J. and Pick J. (1969) Solubility of carbon dioxide in water at pressures up to 40 atm. *Collection of Czechoslovak Chemical Communications* **34**, 3982–2985.

Molnar P., England P. and Martinod J. (1993) Mantle dynamics, uplift of the Tibetan plateau, and the Indian monsoon. *Reviews Of Geophysics* **31**, 357–396. doi:10.1029/93RG02030.

Monica M.D., Ceglie A. and Agostiano A. (1984) A conductivity equation for concentrated aqueous solutions. *Electrochimica Acta* **29**, 933 – 937. doi: 10.1016/0013-4686(84)87138-8.

Müller G., Bender E. and Maurer G. (1988) Vapor-liquid-equilibrium in the ternary-system ammonia-carbon dioxide-water at high water contents in the range 373-K to 473-K. *Berichte der Bunsen-Gesellschaft-Physical Chemistry Chemical Physics* **92**, 148–160.

Namiot A. (1991) Solubility of Gases in Water. *Nedra, Moscow* .

Nesbitt H.W. and Markovics G. (1997) Weathering of granodioritic crust, long-term storage of elements in weathering profiles, and petrogenesis of siliciclastic sediments. *Geochimica et Cosmochimica Acta* **61**, 1653 – 1670. doi: 10.1016/S0016-7037(97)00031-8.

Newton R., Smith J. and Windley B. (1980) Carbonic metamorphism, granulites and crustal growth. *Nature* **288**, 45–50. doi:10.1038/288045a0.

Nicollet C. and Goncalves P. (2005) Two contrasted P-T-time paths of coronitic metanorites of the French Massif Central: are reaction textures reliable guides to metamorphic histories? *Journal of Metamorphic Geology* **23**, 97–105. doi: 10.1111/j.1525-1314.2005.00564.x.

Nighswander J., Kalogerakis N. and Mehrotra A. (1989) Solubilities of carbon-dioxide in water and 1 wt-percent NaCl solution at pressures up to 10-mpa and temperatures from 80 degrees C to 200 degrees C. *Journal of Chemical and Engineering Data* **34**, 355–360.

Oelkers E.H. and Helgeson H.C. (1988) Calculation of the thermodynamic and transport properties of aqueous species at high pressures and temperatures: dissociation constants for supercritical alkali metal halides at temperatures from 400 to 800°C and pressures from 500 to 4000 bar. *The Journal of Physical Chemistry* **92**, 1631–1639. doi:10.1021/j100317a049.

Oelkers E.H. and Helgeson H.C. (1993) Calculation of dissociation constants and the relative stabilities of polynuclear clusters of 1:1 electrolytes in hydrother-

mal solutions at supercritical pressures and temperatures. *Geochimica et Cosmochimica Acta* **57**, 2673 – 2697. doi:10.1016/0016-7037(93)90383-8.

Oelkers E.H., Benezeth P. and Pokrovski G.S. (2009) Thermodynamic Databases for Water-Rock Interaction. In *THERMODYNAMICS AND KINETICS OF WATER-ROCK INTERACTION* (eds. E. Oelkers and J. Schott), Mineralogical Society of America, vol. 70 of *Reviews in Mineralogy & Geochemistry*, pp. 1–46. doi:10.2138/rmg.2009.70.1.

Onsager L. (1927) On the theory of electrolytes. II. *Physikalische Zeitschrift* **28**, 277–298.

Pinho S.P. and Macedo E.A. (2005) Solubility of NaCl, NaBr, and KCl in Water, Methanol, Ethanol, and Their Mixed Solvents. *Journal of Chemical & Engineering Data* **50**, 29–32. doi:10.1021/je049922y.

Pitzer K. (1973) Thermodynamics of electrolytes.1. Theoretical basis and general equations. *Journal of Physical Chemistry* **77**, 268–277.

Pitzer K. and Mayorga G. (1973) Thermodynamics of electrolytes .2. Activity and osmotic coefficients for strong electrolytes with one or both ions univalent. *Journal of Physical Chemistry* **77**, 2300–2308.

Pitzer K., Peiper J. and Busey R. (1984) Thermodynamic properties of aqueous sodium-chloride solutions. *Journal of Physical and Chemical Reference Data* **13**, 1–102.

Pitzer K.S. and Simonson J.M. (1986) Thermodynamics of multicomponent, miscible, ionic systems: theory and equations. *The Journal of Physical Chemistry* **90**, 3005–3009. doi:10.1021/j100404a042.

Pitzer K.S. and Sterner S.M. (1994) Equations of state valid continuously from zero to extreme pressures for H_2O and CO_2. *The Journal of Chemical Physics* **101**, 3111–3116. doi:10.1063/1.467624.

Powell R., Holland T.J.B. and Worley B. (1998) Calculating phase diagrams involving solid solutions via non-linear equations, with examples using THERMOCALC. *Journal of Metamorphic Geology* **16, 4**, 577–588. doi: 10.1111/j.1525-1314.1998.00157.x.

Quist A.S. and Marshall W.L. (1968) Electrical conductances of aqueous sodium chloride solutions from 0 to 800°C and at pressures to 4000 bars. *Journal of Physical Chemistry* **72**, 684–703. doi:10.1021/j100848a050.

Rumpf B., Nicolaisen H., Ocal C. and Maurer G. (1994) Solubility of carbon dioxide in aqueous solutions of sodium chloride: Experimental results and Correlation. *Journal of Solution Chemistry* **23**, 431–448.

Sander W. (1912) On the solubility of carbon acid in water and some other solutions under high pressure. *Zeitschrift Fur Physikalische Chemie–Stochiometrie Und Verwandtschaftslehre* **78**, 513–549.

Santosh M. and Omori S. (2008) CO_2 flushing: A plate tectonic perspective. *Gondwana Research* **13**, 86 – 102. doi:10.1016/j.gr.2007.07.003.

Sawamura S., Egoshi N., Setoguchi Y. and Matsuo H. (2007) Solubility of sodium chloride in water under high pressure. *Fluid Phase Equilibria* **254**, 158 – 162. doi:10.1016/j.fluid.2007.03.003.

Seidell A. (1940) *Solubilities of inorganic and metal organic compounds.* DVan Nostrand Company, New York.

Servio P. and Englezos P. (2001) Effect of temperature and pressure on the solubility of carbon dioxide in water in the presence of gas hydrate. *Fluid Phase Equilibria* **190**, 127 – 134. doi:10.1016/S0378-3812(01)00598-2.

Sharygin A.V., Wood R.H., Zimmerman G.H. and Balashov V.N. (2002) Multiple Ion Association versus Redissociation in Aqueous NaCl and KCl at High Temperatures. *The Journal of Physical Chemistry B* **106**, 7121–7134. doi: 10.1021/jp013647u.

Shedlovsky T. (1938) The computation of ionization constants and limiting conductance values from conductivity measurements. *Journal of the Franklin Institute* **225**, 739 – 743. doi:10.1016/S0016-0032(38)90931-7.

Sherman D.M. and Collings M.D. (2002) Ion association in concentrated NaCI brines from ambient to supercritical conditions: results from classical molecular dynamics simulations. *Geochemical Transactions* **3**, 102–107. doi: 10.1186/1467-4866-3-102.

Spear F. (1993) *Metamorphic Phase Equilibria and Pressure-Temperature-Time Paths*. Mineralogical Society of America, Washington, D. C.

Spycher N., Pruess K. and Ennis-King J. (2003) CO_2-H_2O mixtures in the geological sequestration of CO_2. I. Assessment and calculation of mutual solubilities from 12 to 100°C and up to 600 bar. *Geochimica et Cosmochimica Acta* **67**, 3015 – 3031. doi:10.1016/S0016-7037(03)00273-4.

Sterner S. and Bodnar R. (1991) Synthetic fluid inclusions.X: Experimental determination of P-V-T-X properties in the CO_2-H_20 system to 6 kb and 700 °C. *American Journal of Science* **291**, 1–54.

Sterner S. and Pitzer K. (1994) An Equation Of State For Carbon-Dioxide Valid From Zero To Extreme Pressures. *Contributions to Mineralogy and Petrology* **117**, 362–374.

Stewart P.B. and Munjal P.K. (1970) Solubility of carbon dioxide in pure water, synthetic sea water, and synthetic sea water concentrates at -5deg. to 25deg. and 10- to 45-atm. pressure. *Journal of Chemical & Engineering Data* **15**, 67–71. doi:10.1021/je60044a001.

Surdo A.L., Alzola E.M. and Millero F.J. (1982) The (p, V, T) properties of concentrated aqueous electrolytes I. Densities and apparent molar volumes of NaCl, Na_2SO_4, $MgCl_2$, and $MgSO_4$ solutions from 0.1 molkg-1 to saturation and from 273.15 to 323.15 K. *The Journal of Chemical Thermodynamics* **14**, 649 – 662. doi:10.1016/0021-9614(82)90080-5.

Takenouchi S. and Kennedy G. (1965) Solubility of carbon dioxide in NaCl solutions at high temperatures and pressures. *American Journal of Science* **263**, 445–454.

Takenouchi S. and Kennedy G.C. (1964) The bynary system H_2O-CO_2 at high temperatures and pressures. *American Journal of Science* **262**, 1055–1074.

Tatsumi Y. (1989) Migration of fluid phases and genesis of basalt magmas in subduction zones. *Journal of Geophysical Research* **94**, 4697–4707. doi: 10.1029/JB094iB04p04697.

Teng H., Yamasaki A., Chun M.K. and Lee H. (1997) Solubility of liquid CO_2 in water at temperatures from 278 K to 293 K and pressures from 6.44 MPa to

29.49 MPa and densities of the corresponding aqueous solutions. *The Journal of Chemical Thermodynamics* **29**, 1301 – 1310. doi:10.1006/jcht.1997.0249.

Thompson A. (1992) Water in the Earth's upper mantle. *Nature* **358**, 295–302. doi:10.1038/358295a0.

Thompson J.B.J. (1967) *Thermodynamic properties of simple solutions*. John Wiley and Sons, New York.

Tipper E., Galy A., Gaillardet J., Bickle M., Elderfield H. and Carder E. (2006) The magnesium isotope budget of the modern ocean: Constraints from riverine magnesium isotope ratios. *Earth and Planetary Science Letters* **250**, 241 – 253. doi:10.1016/j.epsl.2006.07.037.

Todheide K. and Franck E.U. (1963) Das Zweiphasengebiet die kritische Kurve im System Kohlendioxid-Wasser bis zu Drucken von 3500 bar. *Zeitschrift für Physikalische Chemie (Neue Folge)* **37**, 387 – 401.

Vidal O. and Dubacq B. (2009) Thermodynamic modelling of clay dehydration, stability and compositional evolution with temperature, pressure and H_2O activity. *Geochimica et Cosmochimica Acta* **73**, 6544 – 6564. doi:10.1016/j.gca.2009.07.035.

Vilcu R. and Gainar I. (1967) Löslichkeit Der Gase Unter Druck In Flüssigkeiten .I. Das System Kohlendioxid-Wasser. *Revue Roumaine de Chimie* **12**, 181–189.

White R., Powell R. and Holland T. (2001) Calculation of partial melting equilibria in the system Na_2O-CaO-K_2O-FeO-MgO-Al_2O_3-SiO_2-H_2O (NCKF-MASH). *Journal of Metamorphic Geology* **19**, 139–153. doi:10.1046/j.0263-4929.2000.00303.x.

1292 Wiebe R. and Gaddy V.L. (1939) The Solubility in Water of Carbon Dioxide at
1293 50, 75 and 100°C, at Pressures to 700 Atmospheres. *Journal of the American*
1294 *Chemical Society* **61**, 315–318.

1295 Wiebe R. and Gaddy V.L. (1940) The Solubility of Carbon Dioxide in Water at
1296 Various Temperatures from 12 to 40°C and at Pressures to 500 Atmospheres.
1297 Critical Phenomena. *Journal of the American Chemical Society* **62**, 815–817.

1298 Wigley M., Kampman N., Dubacq B. and Bickle M.J. (2012) Fluid-mineral reac-
1299 tions and trace metal mobilization in an exhumed natural CO_2 reservoir, Green
1300 River, Utah. *Geology* **40**, 555–558. doi:10.1130/G32946.1.

1301 Wilkinson J.J. and Johnston J.D. (1996) Pressure fluctuations, phase separation,
1302 and gold precipitation during seismic fracture propagation. *Geology* **24**, 395–
1303 398. doi:10.1130/0091-7613(1996)024<0395:PFPSAG>2.3.CO;2.

1304 Wishaw B.F. and Stokes R.H. (1954) The Diffusion Coefficients and Conduc-
1305 tances of Some Concentrated Electrolyte Solutions at 25°C. *Journal of the*
1306 *American Chemical Society* **76**, 2065–2071. doi:10.1021/ja01637a011.

1307 Yang S., Yang I., Kim Y. and Lee C. (2000) Measurement and prediction of phase
1308 equilibria for water+CO_2 in hydrate forming conditions. *Fluid Phase Equilibria*
1309 **175**, 75 – 89. doi:10.1016/S0378-3812(00)00467-2.

1310 Zakirov I., Sretenskaja N., Aranovich L. and Volchenkova V. (2007) Solubil-
1311 ity of NaCl in CO_2 at high pressure and temperature: First experimental
1312 measurements. *Geochimica et Cosmochimica Acta* **71**, 4251 – 4255. doi:
1313 10.1016/j.gca.2007.01.028.

1314 Zawisza A. and Malesinska B. (1981) Solubility of carbon-dioxide in liquid water
1315 and of water in gaseous carbon-dioxide in the range 0.2-5 MPa and at tempera-
1316 tures up to 473-K. *Journal of Chemical and Engineering Data* **26**, 388–391.

1317 Zelvinskii Y. (1937) Measurements of carbon dioxide solubility in water. (in Rus-
1318 sian). *Zhurn. Khim. Prom.* **14**, 1250–1257.

Symbol	Quantity
R	Ideal gas constant ($= 8.314472$ J.mol^{-1}.K^{-1})
T	Temperature
P	Pressure
STP	Standard temperature and pressure, 298.15K and 1 bar
T_{C}, x_{C}	Critical temperature and composition
μ_i	Chemical potential of end-member i
μ_i^0	Standard state chemical potential of i
x_i	Mole fraction of i
γ_i	Activity coefficient of i
a_i	Activity of i: $\mathrm{a}_i = x_i.\gamma_i$
σ_i^2	Variance of i
$\overline{G}_{\mathrm{m}}^{\mathrm{mix}}(x)$	Gibbs free energy of mixing
$\overline{G}_{\mathrm{m}}(x)$	Gibbs free energy of the mixture
$\overline{G}_{\mathrm{m}}^{\mathrm{xs}}(x)$	Excess Gibbs free energy of the mixture
Φ_i	Proportion of i adjusted to a size parameter
W_{ij}^*	Interaction energy between i and j adjusted to a size parameter
W_j	Interaction energy between i and j
α_i	Size parameter for i
W_G, W_H, W_S, W_V	Interaction parameters on the Gibbs free energy, enthalpy, entropy and volume of mixing, respectively.
$\Lambda\epsilon$, Λe	Equivalent conductance, respectively experimentally-determined and hypothetical from a completely dissociated electrolyte
Λe^0	Limiting equivalent conductance
η, η_0	Viscosity, respectively of the solution and of the pure solvent
ρ	Density of the solution
ϵ	Dielectric constant of water
$\mathring{a}$	Ion size parameter

Table 1: Key to symbols used in the text.

Reference	Pressure - temperature range
Adams (1931)	25°C, 1-4 kbar
Compilation of data from Seidell (1940)	20-300°C, 1-4 kbar
Keevil (1942)	180-650°C, water vapor pressure
Clynne et al. (1981)	26-94°C, 1 bar
Farelo et al. (1993)	20-80°C, 1 bar
Pinho and Macedo (2005)	25-80°C, 1 bar
Sawamura et al. (2007)	20-40°C, 1-3 kbar

Table 2: Selected experimental results of halite solubility.

P bars	T °C	molality CO_2	ρ_{Meas}	ρ_{Calc}	Deviation ‰
10	25	0.155	996.9	970.7	26.2
200	25	0.155	1005.3	1005.0	0.3
200	50	0.155	996.0	996.5	-0.5
200	100	0.155	966.5	965.8	0.7
200	150	0.155	926.4	926.7	-0.4
200	200	0.155	875.9	879.1	-3.7
200	250	0.185	813.4	821.0	-9.4
200	300	0.155	731.1	740.2	-12.4
280	350	0.155	631.7	642.1	-16.4
350	25	0.155	1011.7	1011.4	0.3
350	50	0.155	1002.2	1002.4	-0.2
350	100	0.155	973.1	973.9	-0.8
350	150	0.155	934.1	934.7	-0.6
350	200	0.155	885.9	887.2	-1.4
350	250	0.185	827.7	831.3	-4.4
350	300	0.155	754.7	760.6	-7.8
197	10	1.741	1020.8	1016.4	-4.2
246	10	1.796	1021.7	1020.5	-1.2
295	10	1.840	1024.0	1023.0	-1.0
197	15	1.702	1019.7	1015.8	-3.8
246	15	1.757	1021.0	1019.6	-1.3
295	15	1.801	1022.9	1022.0	-0.9
197	20	1.614	1017.7	1015.0	-2.7
246	20	1.675	1019.1	1019.0	-0.1
295	20	1.719	1019.8	1021.4	1.6

Table 3: Comparison of measured (ρ_{Meas}) and calculated (ρ_{Calc}) densities at various pressures, temperatures and CO_2 concentrations. Measurements at CO_2 concentrations around 0.15 M originate from Hnedkovský et al. (1996), and measurements above 1M CO_2 are taken from Teng et al. (1997).

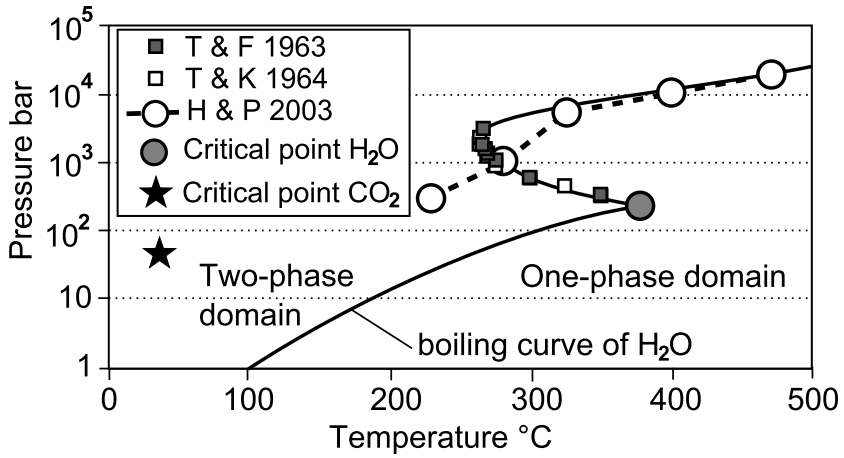

Figure 1: Phase diagram for CO_2-H_2O mixtures. Note that pressure is on a logarithmic scale. T&F 1963: Measurements of Todheide and Franck (1963). T&K1964: Measurements of Takenouchi and Kennedy (1964). H&P 2003: Model of Holland and Powell (2003). High pressure - low temperature solid phases (ices and clathrates) are not represented.

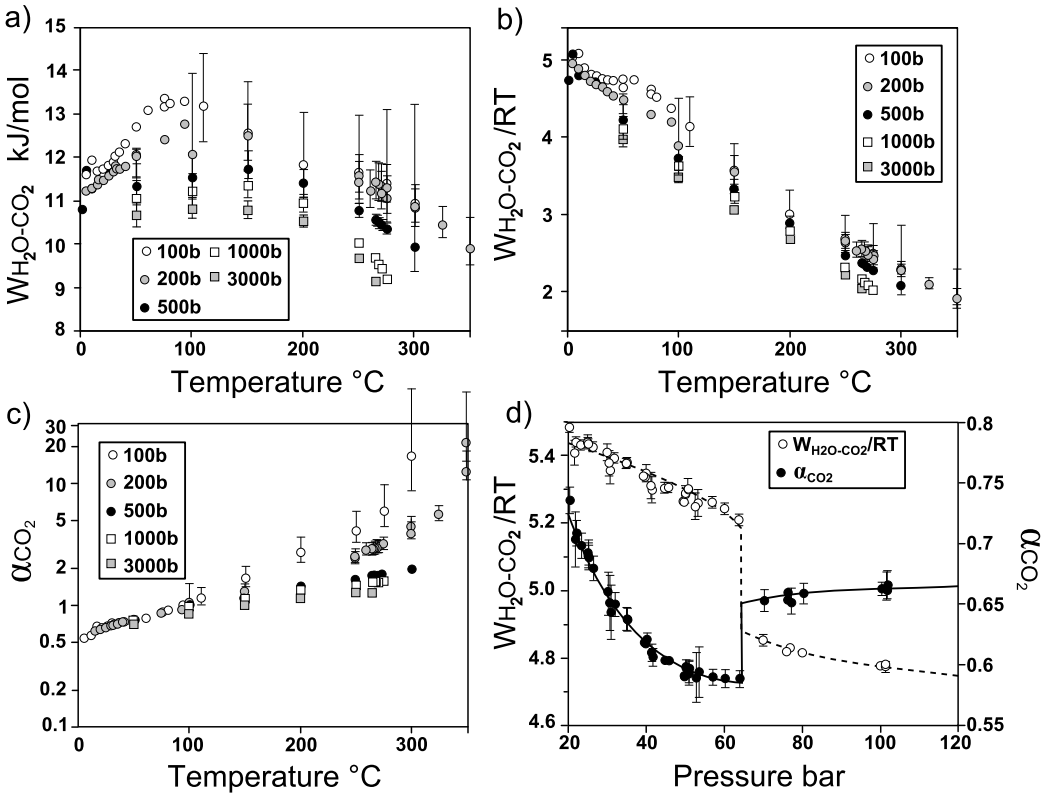

Figure 2: Representative values of $W_{\mathrm{H_2O\text{-}CO_2}}$ and $a_{\mathrm{CO_2}}$ from selected experimental results. a) and b) respectively show isobaric values of $W_{\mathrm{H_2O\text{-}CO_2}}$ and $W_{\mathrm{H_2O\text{-}CO_2}}/\mathrm{RT}$ as a function of temperature. c) Isobaric values of $a_{\mathrm{CO_2}}$ as a function of temperature. Note the log scale to represent low pressure value of $a_{\mathrm{CO_2}}$. d) Variations of $W_{\mathrm{H_2O\text{-}CO_2}}$ (open symbols and dashed lines) and $a_{\mathrm{CO_2}}$ (closed symbols and plain lines) with pressure at 25°C. A step is seen at the boiling curve of CO_2. Lines are calculated wih eq. 8 and 9. Uncertainties are smaller than the size of the point when not indicated.

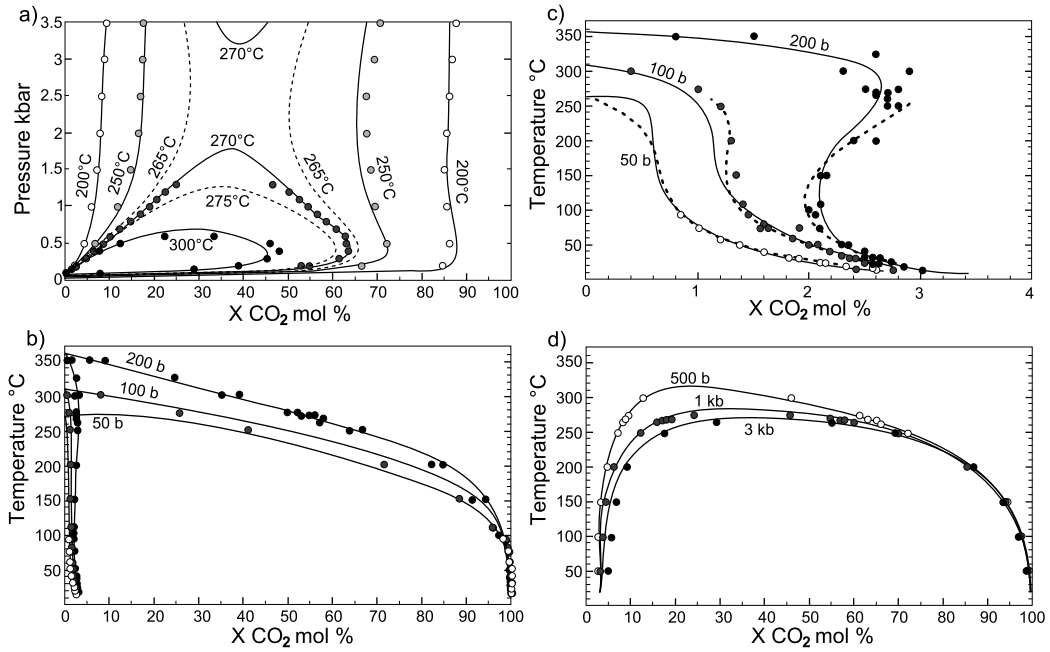

Figure 3: Phase equilibrium in the H_2O-CO_2 system at various pressures and temperatures (cross-sections through figure 1). Lines are calculated and points are experimental results at the pressure - temperature corresponding to the lines closest to which they plot. a) Pressure-composition phase diagram at different temperatures. The solvus closes at low pressure against the boiling curve of water (X CO_2 $=$ 0). Dashed lines illustrate the dependency of the phase diagram to temperatures around 270°C. Corresponding experimental measurements are not indicated for clarity. b), c) and d) show temperature-composition phase diagrams at different pressures. c) is a close-up view of b) for the water-rich phase. Dotted lines are calculated with the model of Duan and Sun (2003).

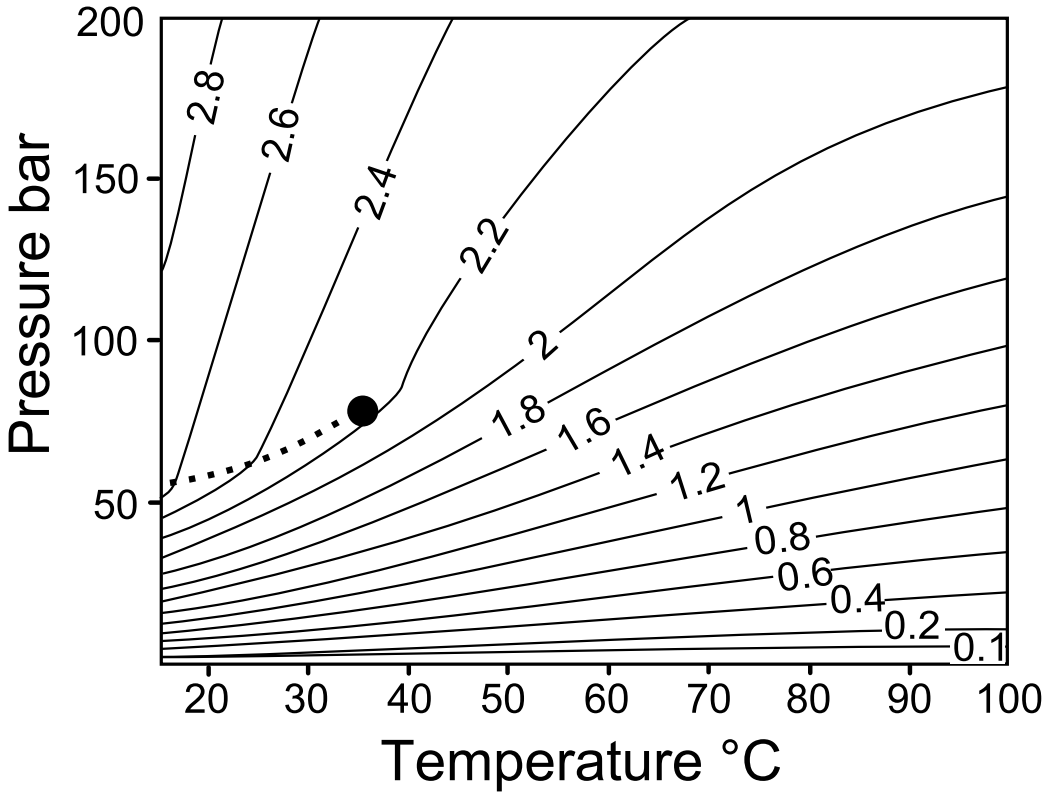

Figure 4: a) Isopleths of calculated CO_2 solubility (mol. %) in pure water at low pressures and temperatures. The dark circle indicates the critical point of CO_2 and the dashed line is the liquid-gas transition of CO_2.

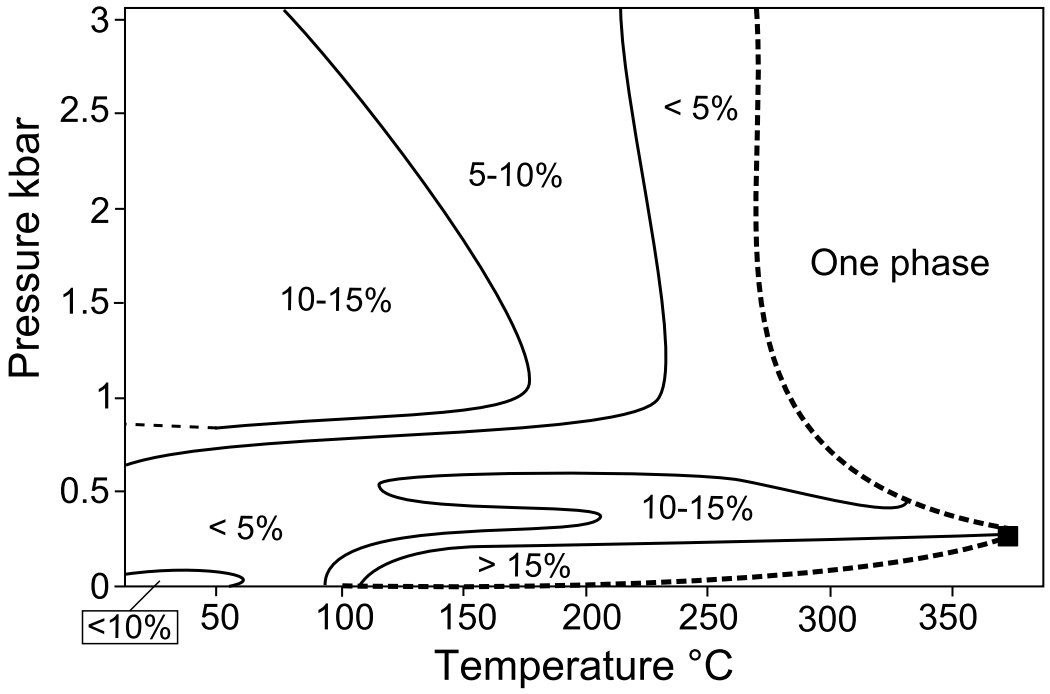

Figure 5: Map of uncertainties on CO_2 solubility, in percent of the calculated value. This map takes into account experimental uncertainties and the misfit of the model to the data.

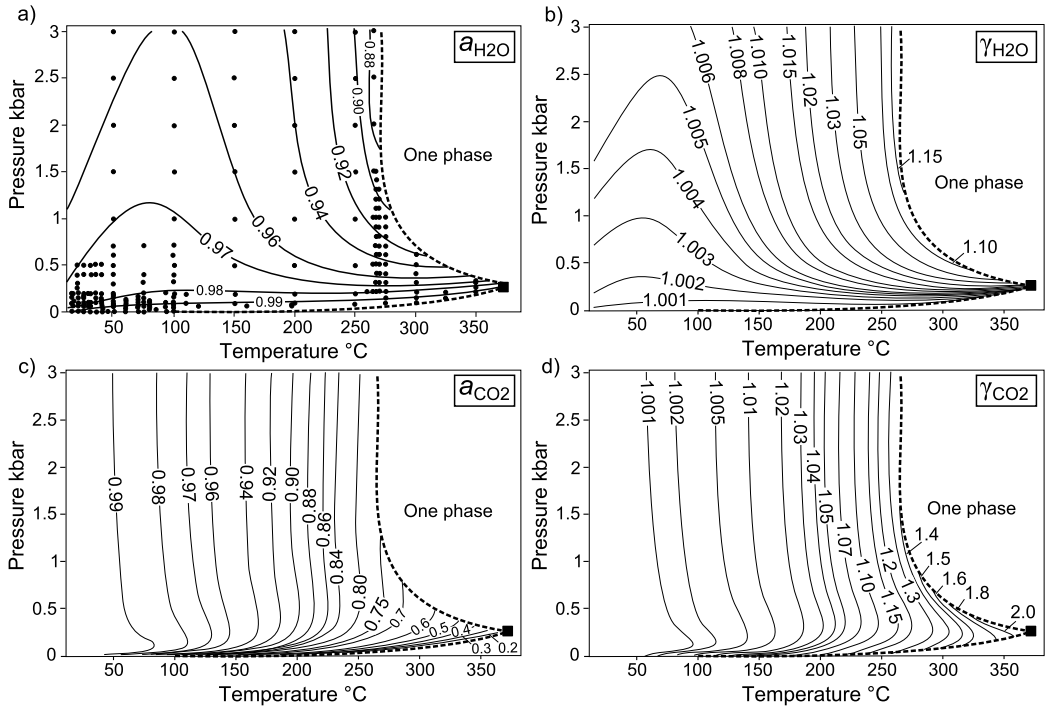

Figure 6: Isopleths of calculated a) water activity (a_{H_2O}) and b) water activity coefficient (γ_{H_2O}) in CO_2-saturated solutions, c) CO_2 activity (a_{CO_2}) and d) CO_2 activity coefficient (γ_{CO_2}) in the water-saturated CO_2-rich phase, between 25 and 380°C and 1 bar to 3 kbar. Dashed curves illustrate the two critical mixing lines. Points in a) represent pressure-temperature conditions of experimental results used in this study. The square indicates the critical point of water.

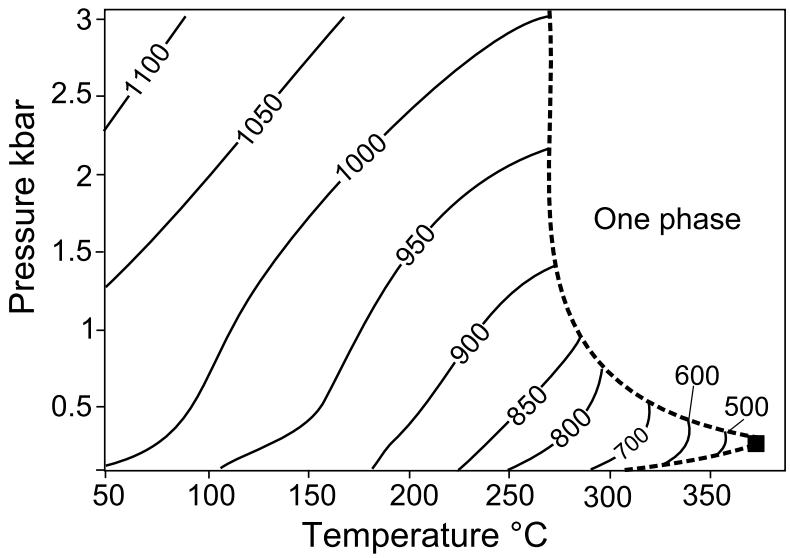

Figure 7: Calculated density isopleths of the CO_2-saturated aqueous phase over the range 0.1-3kb and 50-370°C, in kg.m^{-3}.

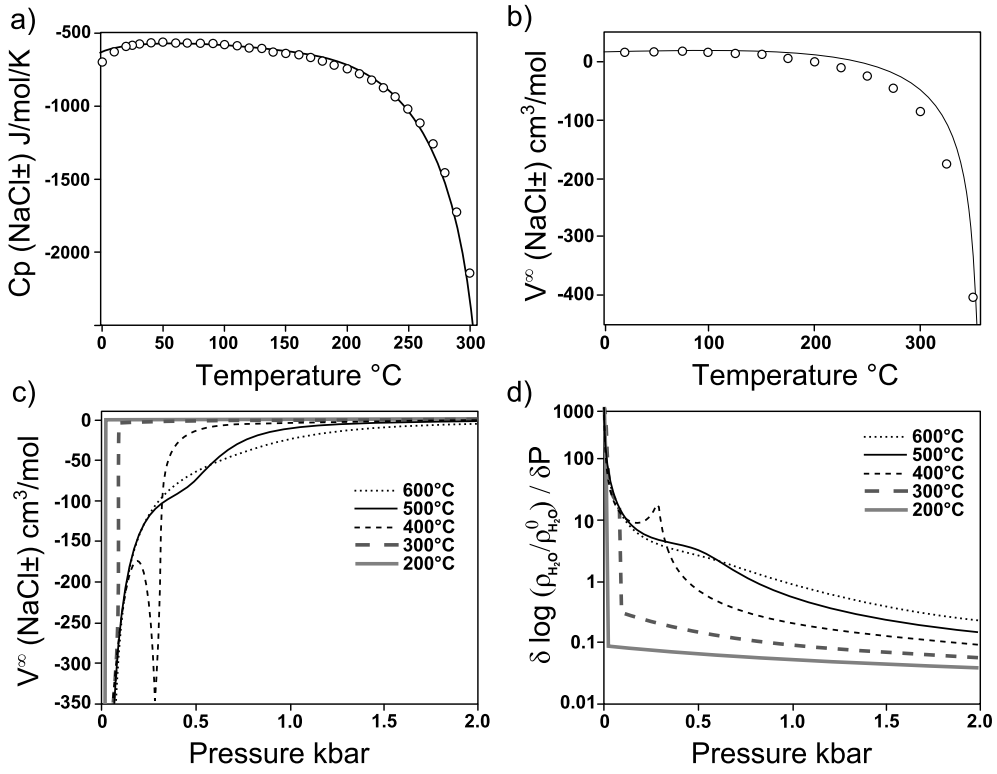

Figure 8: Heat capacity (Cp) and volume of NaCl± at infinite dilution (V^{∞}) calculated with the modified density model (Holland and Powell, 1998). a) Heat capacity at 200 bars compared to measurements from Pitzer et al. (1984). b) Comparison with the experimentally-derived volumes of Grant-Taylor (1981) and L'Vov et al. (1981). c) Isotherms of calculated V^{∞}(NaCl±) up to 2 kbars. d) Isotherms of the pressure derivative of $\ln(\rho_{H_2O}/\rho^0_{H_2O})$, plotted on a log scale and used in the calculation of V^{∞}(NaCl±).

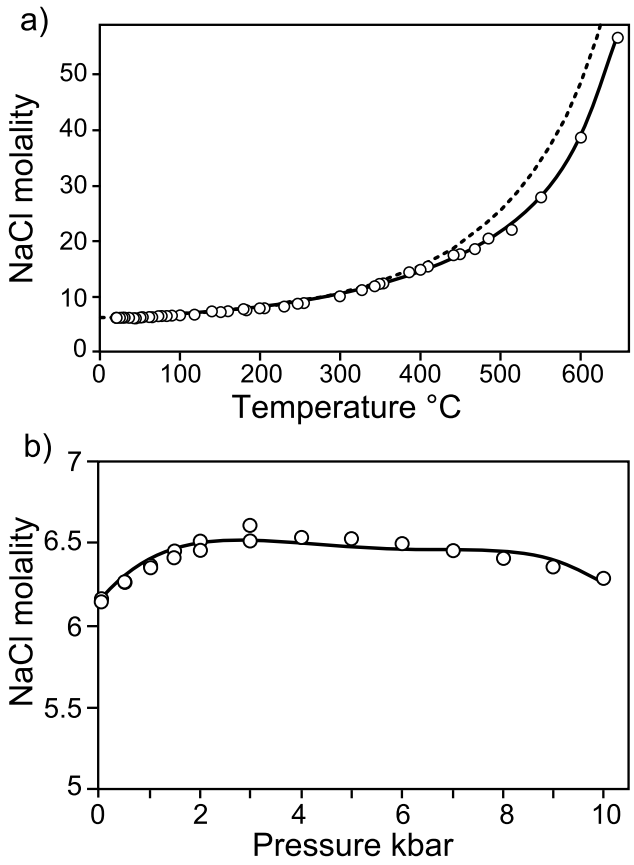

Figure 9: a) Solubility of halite calculated as a function of temperature with the model of Mao and Duan (2008, dotted line) and with the present model (bold line). The solubility is calculated at water vapor pressure below the critical point of water and along a linear pressure gradient linking experimental pressures above the critical point of water. b) Solubility of halite calculated at 25°C as a function of pressure. Points are experimental measurements indicated in table 2.

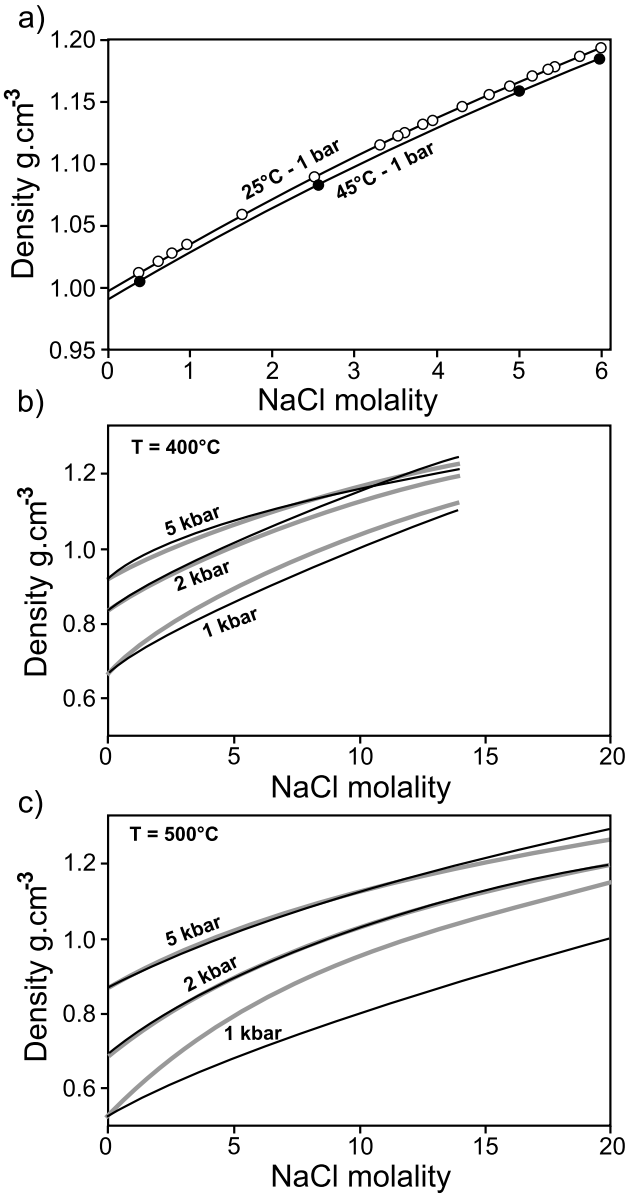

Figure 10: a) Density of NaCl solutions calculated at 1 bar (dark line) compared to the measurements of Surdo et al. (1982) at 25°C (open symbols) and 45°C (closed symbols). b) and c): density of NaCl solutions calculated at 400 and 500 °C for various pressures with this model (dark lines) and with the model of Driesner (2007) (thick gray lines).

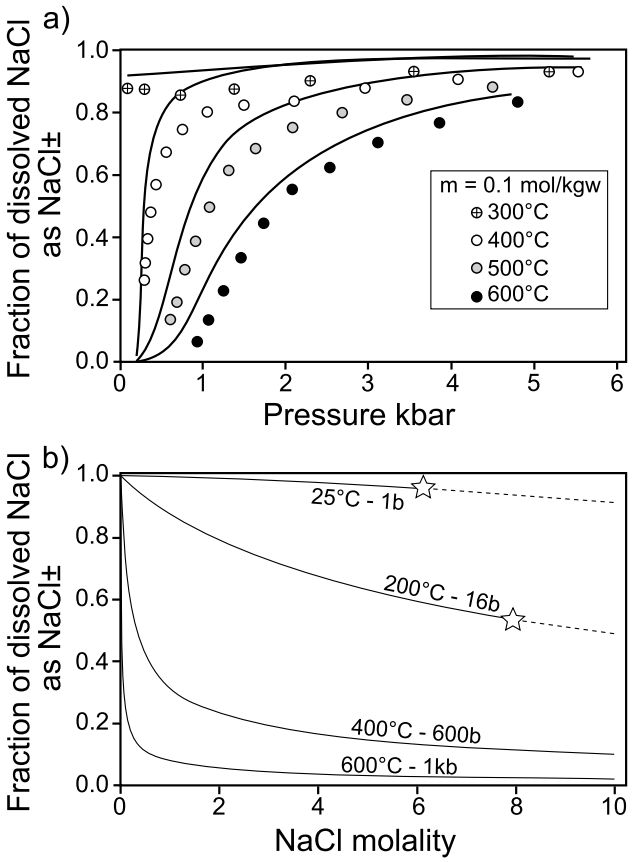

Figure 11: a) Fraction of dissociated aqueous NaCl ($x_{\mathrm{NaCl}\pm}$) as a function of pressure, calculated at different temperatures and compared to the degree of association calculated from the conductivity measurements of Quist and Marshall (1968) at 0.1 molal, as described in the text. b) $x_{\mathrm{NaCl}\pm}$ calculated as a function of the total concentration of NaCl for various pressures and temperatures. The fraction of NaCl^0 is $x_{\mathrm{NaCl}^0} = 1 - x_{\mathrm{NaCl}\pm}$. Stars indicate halite saturation.

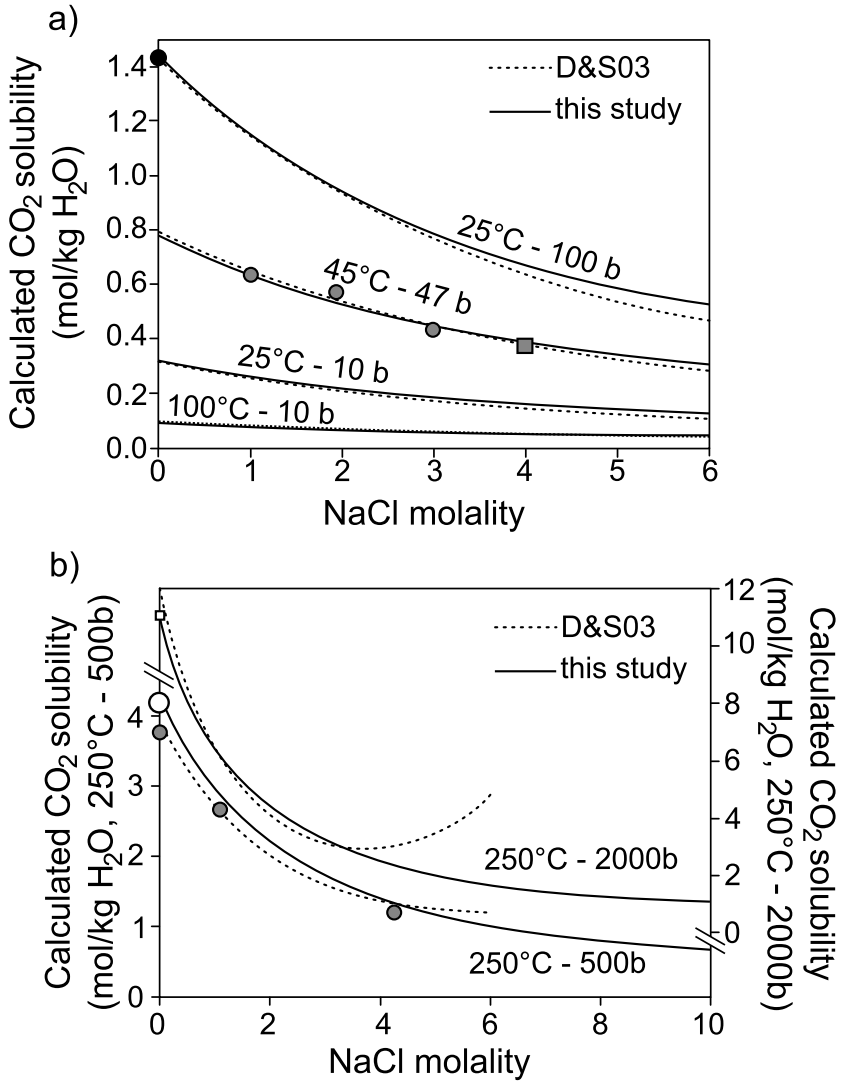

Figure 12: a) Solubility of CO_2 as a function of concentration of NaCl, calculated at indicated pressure and temperatures with the present model and Duan and Sun (2003, dotted line labeled D&S03). Black circle at 25°C: Wiebe and Gaddy (1940). Grayed symbols are measurements of Drummond (1981) between 47 and 48 bars (circles) and at 42 bars (square). b) CO_2 solubility at 250°C calculated at 500 bars (left axis) and 2000 bars (right axis). Grayed circles are measurements of Takenouchi and Kennedy (1965) with unknown uncertainties. Open symbols are measurements of Todheide and Franck (1963) at 500 bars (circle) and 2000 bars (square), whose sizes indicate experimental uncertainty.

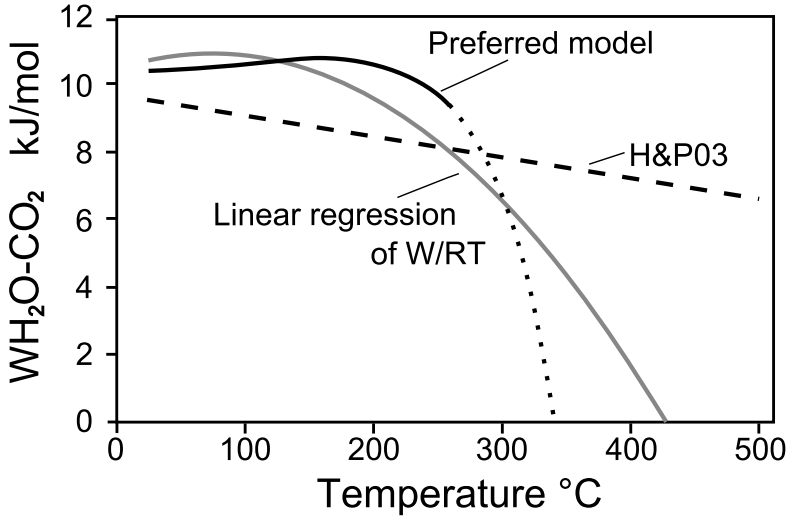

Figure 13: Comparison of values for $W_{\mathrm{H_2O\text{-}CO_2}}$ at 3 kbar given by the model of Holland and Powell (2003, dashed line), by linear regression of $W_{\mathrm{H_2O\text{-}CO_2}}/RT$ (gray line, see section 2.2) and by the model proposed in this study, in the two-phase domain (plain line) and extrapolated in the one-phase domain (dotted line).